TABLE OF CONTENTS

New Performance Results for QAM OFDM RoFSO Over K and Exponentially Modeled Turbulence Channels

H.E. Nistazakis[a], M.P. Ninos[a], A.N. Stassinakis[a],
A.D. Tsigopoulos[b], and G.S. Tombras[a]

[a]Department of Electronics, Computers, Telecommunications and Control, Faculty of
Physics, National and Kapodistrian University of Athens, Athens, 15784, Greece
e-mails: {enistaz; ninmichail; a-stasinakis; gtombras}@phys.uoa.gr
[b]Section of Battle Systems, Naval Operations, Sea Studies, Navigation, Electronics and
Telecommunications, Hellenic Naval Academy, Hadjikyriakou ave,
Piraeus 18539, Greece, e-mail: atsigo @snd.edu.gr

Abstract. Free space laser communications are gaining popularity due to their high bandwidth and security transmission that they offer, the license free spectrum use and the sufficient reliability for operational and installation costs compared to RF communication systems. The radio on free space optics (RoFSO) is a technology of modulating RF signals on optical carriers for transmission over the free space. However, the performance of those systems depends strongly on the atmospheric conditions. In this work, we study a RoFSO communication link which is using the orthogonal frequency division multiplexing (OFDM) scheme with quadrature amplitude modulation (QAM) format over the atmospheric turbulence channel, modeled either with K or negative exponential distribution. Using a very recently presented accurate approximation for the Q-function we derive new closed form mathematical expressions for the estimation of the BER and the outage probability of a QAM OFDM RoFSO link over turbulence channels modeled either with the K or the NE distribution. Finally, we investigate the performance of these optical wireless communication systems with numerical results using the derived expressions and realistic link's parameters.

Keywords: BER, Outage Probability, Free Space Optical Communications, OFDM, PSK.

PACS: 42.79.Sz, 42.81-i, 92.60.hk.

I. INTRODUCTION

Free Space Optical (FSO) communication systems has attracted significant research and commercial interest due to their high data rates, high security level without need of licensing fees and tariffs, lower power consumption, ease of portability, quick deployment and lower overall installation and operational costs compared to conventional radio links and fiber optics [1]-[7].

Radio on free space optics (RoFSO) is a technology similar to the radio over fiber (RoF) where the radio frequency signals are transmitted by optical devices wirelessly, excluding the fiber medium [8]-[11]. Despite the great benefits that they render, their efficiency is influenced by the atmospheric conditions and many harmful effects that affect the atmospheric channel can lead to severe signal fading or even outage of the signal. The most important effects are related to the absorption, scattering and refractive index fluctuations. The absorption and scattering processes referred as extinction caused by the air composition from molecules such as water, carbon dioxide, ozone and other aerosol particulate matter usually larger than molecules like particles formed from gaseous emissions, dust, sea-salt particles etc, [1]-[7], [12]-[19].

The refractive index fluctuations in atmosphere represent a serious mitigation factor which is generated by the turbulence effect. This effect is created when changes in temperature cause inhomogeneities in the refractive index of the air in the form of small eddies. The random temporal and spatial variations in the refractive index affect the intensity level at the receiver which fluctuates, as well. These intensity fluctuations, also known as scintillation effect, have been studied extensively and many statistical models have been proposed to model accurately these signal variations. In this work, we assume the K and the negative exponential (NE) distributions which are suitable for strong and saturate turbulence conditions respectively, [3], [9], [17]-[26].

The orthogonal frequency division multiplexing (OFDM) scheme is a special type of multiple subcarrier modulation (MSM) which has been adopted in many digital audio broadcasting services, digital subscriber lines (DSL), wireless local area networks (WLAN), modern cellular mobile networks etc. The subcarrier modulation can be done with the appropriate, for each specific case, scheme, e.g. quadrature amplitude modulation (QAM), phase shift keying modulation (PSK). The OFDM technique offers high spectral efficiency, robustness against frequency selective fading and avoids intersymbol and narrow-band interference. On the other hand, the large number of subcarriers creates undesired high peak to average power ratios (PAPR). The high PAPR combined with associated addition of dc bias to the OFDM signal in order to be applicable to intensity modulation direct detection IM/DD optical systems, cause efficiency reduction due to intermodulation distortions by the nonlinear laser diode LD characteristics of the transmitter, [9], [11], [27]-[32].

As a consequence of the above mentioned phenomena, we study a RoFSO link using a QAM OFDM scheme and taking into account the atmospheric turbulence effect, modeled either with K or NE distribution, we derive new accurate closed form mathematical expressions for the evaluation of its performance by means of the estimation of its average BER and outage probability.

II. THE CHANNEL MODEL

The optical communication system under consideration is a terrestrial QAM OFDM RoFSO communication link under the action of atmospheric turbulence modeled with the K or the NE distribution models. The initial high data rate streams are split into lower rate parallel streams and then transmitted simultaneously by multiple narrow band orthogonal subcarriers. The OFDM signal for N subcarriers, just before the LD after up conversion to the carrier frequency f_c, is given as, [9]:

$$s_{OFDM}(t) = \sum_{n=0}^{N-1} s_n(t) = \sum_{n=0}^{N-1} X_n \exp\left[i\left(\omega_n + 2\pi f_c\right)t\right] \quad for \ 0 \le t < T_s \tag{1}$$

where each orthogonal subcarrier has an angular frequency of $\omega_n=2\pi n/T_s$, $n=0,\dots,N\text{-}1$, T_s is the OFDM symbol duration and X_n represents the complex data symbol of the n_{th} subcarrier which is mapped according to the selected modulation format which in our case is the QAM scheme. The transmitted optical power $P(t)$ is formulated as follows, [9]:

$$P(t) = P_t\left[1 + \sum_{n=0}^{N-1} m_n s_n(t) + a_3\left(\sum_{n=0}^{N-1} m_n s_n(t)\right)^3\right] \tag{2}$$

where, P_t, is the average transmitted optical power, a_3 stands for the third order nonlinearity coefficient of the LD and m_n is the optical modulation index (OMI) per subcarrier defined as $m_n=\Delta I/(I_b-I_{th})$, with ΔI being the variation of the laser driving current around a bias point and I_b, I_{th}, stand for the bias and threshold laser currents respectively. The received optical power after the atmospheric propagation is $P_r(t)=P(t)L_{tot}I+n(t)$, where L_{tot} is the overall attenuation factor which encompasses the beam extinction from scattering and absorption, misalignment losses and losses due to scintillation. The additive white Gaussian noise (AWGN) of the channel is characterized as $n(t)$ and I is the instantaneous normalized irradiance arriving at the receiver which fluctuates rapidly due to scintillation effect caused by the turbulence. The photo generated current by the impinging power on the avalanche photodiode PD of the receiver is [9]:

$$i(t,I) = I_0\left[1 + \sum_{n=0}^{N-1} m_n s_n(t) + a_3\left(\sum_{n=0}^{N-1} m_n s_n(t)\right)^3\right] + n_{opt}(t) \tag{3}$$

with $I_0=\rho L_{tot}P_t I$ which is the dc of the photo-induced current $i(t,I)$, ρ is the responsivity of the PD, while n_{opt} stands for the optical noise which can be considered as AWGN with zero mean and $N_0/2$ variance, with $N_0=4K_BTF/R_L+2qI_0+I_0^2(RIN)$. In the last expression, K_B is the Boltzmann's constant, T is the temperature, F is the noise figure of the receiver, R_L the load resistor at the PD's side, q the electron charge and RIN is the relative intensity noise from the laser which is a function of the square of the optical power.

Moreover, the effect of intermodulation distortion due to the finite linear operating range of the LD transmitter is another factor that degrades the efficiency of the optical system. The IMD noise for the N subcarriers is as [9], [11]:

$$\sigma_{IMD,n}^2 = \frac{9a_3^2 m_n^6 \rho^2 L_{tot}^2 P_t^2 I^2}{128}\left(2n(N-n+1)+N(N-5)+2-\frac{(-1)^n-(-1)^{2N+n}}{2}\right)^2 \tag{4}$$

The total carrier to noise plus distortion ratio (CNDR) for each subcarrier including the optical noise and the intermodulation distortion, by assuming that the total noise, i.e. IMD and optical noise, are Gaussian distributed [9], [11], and by averaging them scintillation [9], [11], is given as:

$$CNDR_n(I) \approx \frac{m_n^2 \rho^2 L_{tot}^2 P_t^2 I^2}{2\left([N_0/T_S]_{AV} + [\sigma_{IMD}^2]_{AV}\right)} \tag{5}$$

From (5), the average value $[CNDR_n]_{AV}$, can be obtained by averaging the quantities N_0/T_s, σ_{IMD}^2 over I and n respectively and considering that the average value of I is normalized to unity. In this case is given as [9], [11]:

$$[CNDR_n]_{AV} = \frac{(m_n \rho L_{tot} P_t)^2}{2([N_0/T_s]_{AV} + [\sigma^2_{IMD}]_{AV})} \qquad (6)$$

III. THE K AND EXPONENTIALLY MODELED TURBULENCE CHANNEL

The random changes in the refractive index of the atmospheric path are caused by the turbulence effect which can degrade severely the performance of an FSO communication system. Rapid fluctuations on the intensity level at the receiver, the well known scintillations, are related with turbulence induced phenomena like beam spreading out of the transmit path and a continuous random motion of the beam around the receiver's centre. These signal fades create random signal losses or even complete loss of the signal in the case of outage. In order to estimate these signal fluctuations many statistical models have been proposed according to the turbulence strength. In this work we manipulate the K and NE distribution models which are ideal for strong and saturate turbulence conditions respectively. Thus, the probability density function (PDF) for the K distribution model for the normalized irradiance I, is given as, [23]-[25]:

$$f_{K,I}(I) = \frac{2a^{\frac{a+1}{2}}}{\Gamma(a)} I^{\frac{a-1}{2}} K_{a-1}\left(2\sqrt{aI}\right) \qquad (7)$$

While, the corresponding PDF for the NE distribution model has the following form, [22], [26]:

$$f_{NE,I}(I) = \exp(-I) \qquad (8)$$

Moreover, by integrating the expression (7), we conclude to the following cumulative distribution function (CDF) for the K-distribution, [25]:

$$F_{K,I}(I) = \frac{(aI)^{\frac{a+1}{2}}}{\Gamma(a)} G_{1,3}^{2,1}\left(aI \left| \begin{array}{c} 1 - \frac{a+1}{2} \\ \frac{a-1}{2}, \frac{1-a}{2}, -\frac{a+1}{2} \end{array} \right. \right) \qquad (9)$$

while, by integrating (8), we obtain the following CDF for the NE distribution:

$$F_{NE,I}(I) = 1 - \exp(-I) \qquad (10)$$

IV. THE AVERAGE BER

In this section we derive the appropriate expressions for the estimation of a significant performance metric of communication link which is the average BER, [3], [5], [9], [11], [26]. By assuming, Gray code mapping at the transmitter, an accurate expression for the BER estimation of an M-QAM OFDM with N subcarriers is given as, [33]:

$$P_{b,M-QAM} = \frac{1-M^{-1/2}}{N\log_2(M)}\sum_{n=0}^{N-1}\left[2erfc\left(\sqrt{\frac{3CNDR_{n,l}(I)}{2(M-1)}}\right)-\right.$$
$$\left.-\left(1-M^{-1/2}\right)erfc^2\left(\sqrt{\frac{3CNDR_{n,l}(I)}{2(M-1)}}\right)\right] \tag{11}$$

where *erfc(.)*, stands for the complementary error function and *M* is the modulation format parameter of the QAM scheme. By integrating (11), using the suitable PDF according the atmospheric turbulence conditions, over the normalized irradiance, the average BER is estimated as, [11]:

$$P_{b,M-QAM,Av} = \frac{\left(1-M^{-1/2}\right)}{N\log_2(M)}\sum_{n=0}^{N-1}\int_0^\infty\left[2erfc\left(\sqrt{\frac{3CNDR_{n,l}(I)}{2(M-1)}}\right)-\right.$$
$$\left.-\left(1-\sqrt{M^{-1}}\right)erfc^2\left(\sqrt{\frac{3CNDR_{n,l}(I)}{2(M-1)}}\right)\right]f_I(I)dI \tag{12}$$

By substituting (9) or (10) in (12), using the very recently presented accurate approximation for the estimation of the complementary error function, [34], i.e. $erfc(x) \approx \left(5e^{-4x^2}+4e^{-11x^2/10}+e^{-x^2}\right)/12$, and substituting the functions *erfc(.)* and *exp(.)* with the corresponding Meijer ones [35], we solve the integral of (12). Thus, for the case of strong turbulence conditions, i.e. using the PDF of the K-distribution model, we conclude to the following closed form mathematical expression for the estimation of the average BER of the M-QAM OFDM RoFSO link:

$$P_{b,K,M-QAM,AV} = \frac{\left(1-\sqrt{M}^{-1}\right)2^a}{N\pi\Gamma(a)\log_2(M)}\times$$
$$\times\sum_{n=0}^{N-1}\left[\frac{1}{\sqrt{\pi}}\Lambda - \frac{\left(1-\sqrt{M}^{-1}\right)}{288}\left[25\Xi(192)+16\Xi\left(\frac{264}{5}\right)+\right.\right.$$
$$\left.\left.+40\Xi\left(\frac{612}{5}\right)+\Xi(48)+10\Xi(120)+8\Xi\left(\frac{252}{5}\right)\right]\right] \tag{13}$$

where

$$\Xi(x)=G_{4,1}^{1,4}\left(x\delta\left|\begin{matrix}\frac{1-a}{2},\frac{2-a}{2},0,\frac{1}{2}\\0\end{matrix}\right.\right) \text{ and } \Lambda=G_{5,2}^{2,4}\left(24\delta\left|\begin{matrix}\frac{1-a}{2},\frac{2-a}{2},0,0.5,1\\0,0.5\end{matrix}\right.\right) \text{ with } \delta=\frac{[CNDR_n]_{AV}}{a^2(M-1)}.$$

Furthermore, the corresponding expression for the case of the NE distribution is given as:

$$
P_{b,NE,M-QAM,AV} = \frac{2\left(1-\sqrt{M}^{-1}\right)}{N\pi\log_2(M)} \times
$$

$$
\times \sum_{n=0}^{N-1}\left[\Omega - \frac{\sqrt{\pi}\left(1-\sqrt{M}^{-1}\right)}{288}\left[25\Psi(48)+16\Psi\left(\frac{66}{5}\right)+ \right.\right. \tag{14}
$$

$$
\left.\left. +40\Psi\left(\frac{153}{5}\right)+\Psi(12)+10\Psi(30)+8\Psi\left(\frac{63}{5}\right)\right]\right]
$$

with

$$
\Omega = G_{3,2}^{2,2}\left(\frac{6[CNDR_n]_{AV}}{(M-1)}\left|\begin{array}{c}0,\,0.5,\,1\\0,0.5\end{array}\right.\right) \text{ and } \Psi(x)=G_{2,1}^{1,2}\left(\frac{x[CNDR_n]_{AV}}{(M-1)}\left|\begin{array}{c}0,0.5\\0\end{array}\right.\right).
$$

It should be mentioned here, that the above derived new closed form expression obtained in (14) is a more accurate and different than the one obtained from [11] and [36].

IV. THE OUTAGE PROBABILITY

A significant metric for the reliability estimation of the optical link, is the outage probability. This quantity shows the probability of the CNDR at the receiver falls below a critical value which is the threshold of the receiver. In this case the link cannot work and the information signal cannot be recognized by the receiver, [3], [5], [9], [15], [26]. The atmospheric turbulence leads to fast and large irradiance fluctuations which could decrease significantly the value of the instantaneous normalized irradiance, I, at the receiver and fall below the critical threshold I_{th} defined by the receiver's sensitivity. Thus, the outage probability for an OFDM RoFSO link is given as [9]:

$$
P_{out} = \frac{1}{N}\sum_{n=0}^{N-1}P_{out,n} =
$$

$$
= \frac{1}{N}\sum_{n=0}^{N-1}\Pr\left(I_n < I_{n,th}\right) = \frac{1}{N}\sum_{n=0}^{N-1}F_{I_n}\left(I_{n,th}\right) \tag{15}
$$

where $CNDR_n$ and $CNDR_{n,th}$, is the instantaneous and the threshold carrier to noise plus distortion ratio for the n_{th} OFDM subcarrier of the RoFSO link. Using equations (9), (10) with a transformation we express the CDFs as a function of $CNDR_n$. Hence the outage probability is given as:

$$P_{out} = \frac{1}{N} \sum_{n=0}^{N-1} F_{CNDR_n} \left(\sqrt{\frac{CNDR_{n,th}}{[CNDR_n]_{AV}}} \right) \tag{16}$$

Next, from (9) and (16), the final closed form expression for the estimation of the outage probability of the OFDM RoFSO link under strong turbulence conditions, i.e. modeled with the K-distribution model which can be obtained from the gamma gamma [9], is given as:

$$P_{out,K} = \frac{1}{N} \sum_{n=0}^{N-1} \left[\frac{\left(a \sqrt{\frac{CNDR_{n,th}}{[CNDR_n]_{AV}}} \right)^{\frac{a+1}{2}}}{\Gamma(a)} G_{1,3}^{2,1} \left(a \sqrt{\frac{CNDR_{n,th}}{[CNDR_n]_{AV}}} \, \middle| \, \begin{array}{c} 1 - \frac{a+1}{2} \\ \frac{a-1}{2}, \frac{1-a}{2}, -\frac{a+1}{2} \end{array} \right) \right] \tag{17}$$

It should be mentioned here, that the above expression (17), can be easily obtained from the corresponding expression for the gamma gamma distribution model, derived in [9].

Furthermore, by substituting (10) in (16) we conclude to the new derived expression for outage probability of an OFDM RoFSO link over atmospheric turbulence channels modeled with the NE distribution:

$$P_{out,NE} = \frac{1}{N} \sum_{n=0}^{N-1} \left[1 - \exp\left(-\sqrt{\frac{CNDR_{n,th}}{[CNDR_n]_{AV}}} \right) \right] \tag{18}$$

V. NUMERICAL RESULTS

In this section we present numerical results for the average BER and outage probability metrics of the M-QAM OFDM RoFSO communication link. Thus, we assume two $CNDR_{n,th}$ values i.e. 0 and 2 dB for the receiver's sensitivity, two values for the number of the OFDM subcarriers N, i.e. 2000 and 3000, two values for the QAM signal constellation M i.e. 16 and 64, and three values for the K distribution parameter α, i.e. 3, 5 and 7. The other system's parameters that concern the operation of the optical link are the OFDM symbol duration and are fixed to the following values, T_s = 1 ms, P_t = 20dBm, L_{tot} = 20 dB, while the detector's responsivity and the load resistor are equal to 0.8 A/W and 50 Ω, respectively. The relative intensity noise is -130 dB/Hz, the absolute temperature, T_{abs}, is 300 K and the third order nonlinear parameter for the inter-modulation distortion, α_3, is 9×10^{-4}, [9], [11].

It is worth mentioning here, that the above values has been chosen because are common for such OFDM RoFSO communication systems. However, results can be obtained, using the above derived expressions for any other value of the system's parameters which can be supported by the two above mentioned distributions. Further results for other parameters values, e.g. wavelength, link length, etc, can be obtained using other distribution models such as gamma gamma, log normal, etc, [11], [15], [19].

From the figures that follow, we can conclude that the atmospheric conditions affect significantly the performance of the optical communication system. The atmospheric turbulence is modeled with K and NE distributions in order to simulate the irradiance fluctuations at the receiver which correspond to strong and saturate turbulence conditions, respectively.
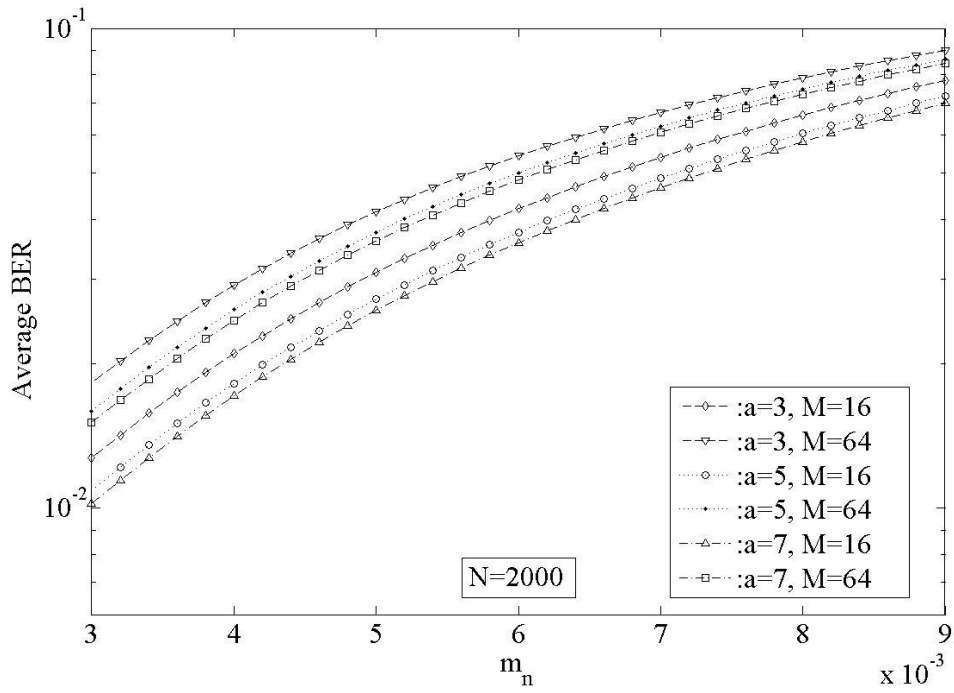
FIGURE 1. Average BER for the cases of strong turbulence conditions, i.e. using the K-distribution model.
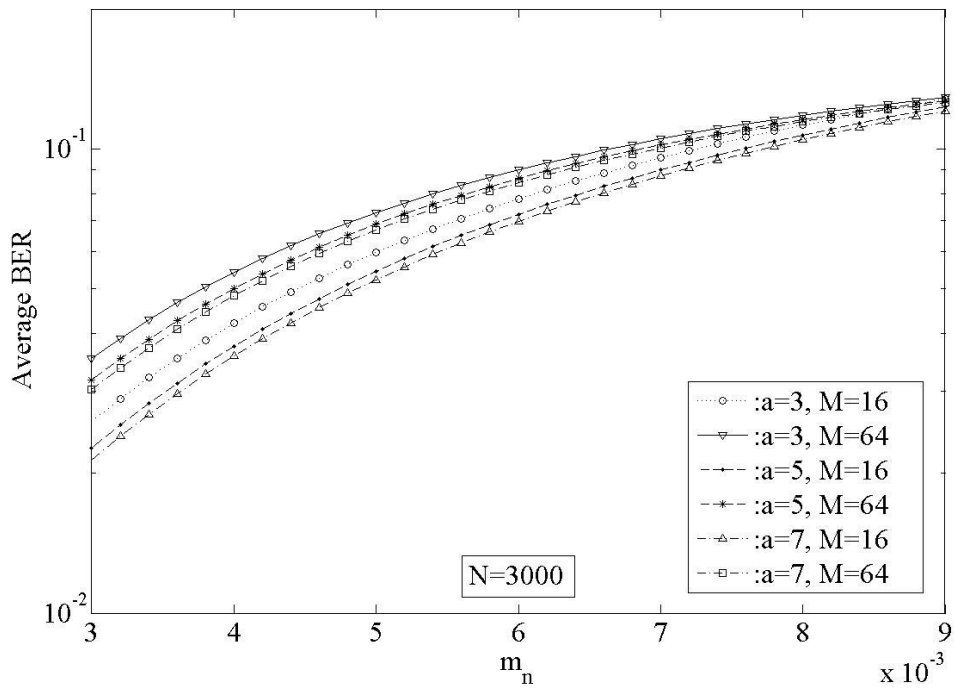

FIGURE 2. Average BER for the cases of strong turbulence conditions, i.e. using the K-distribution model.
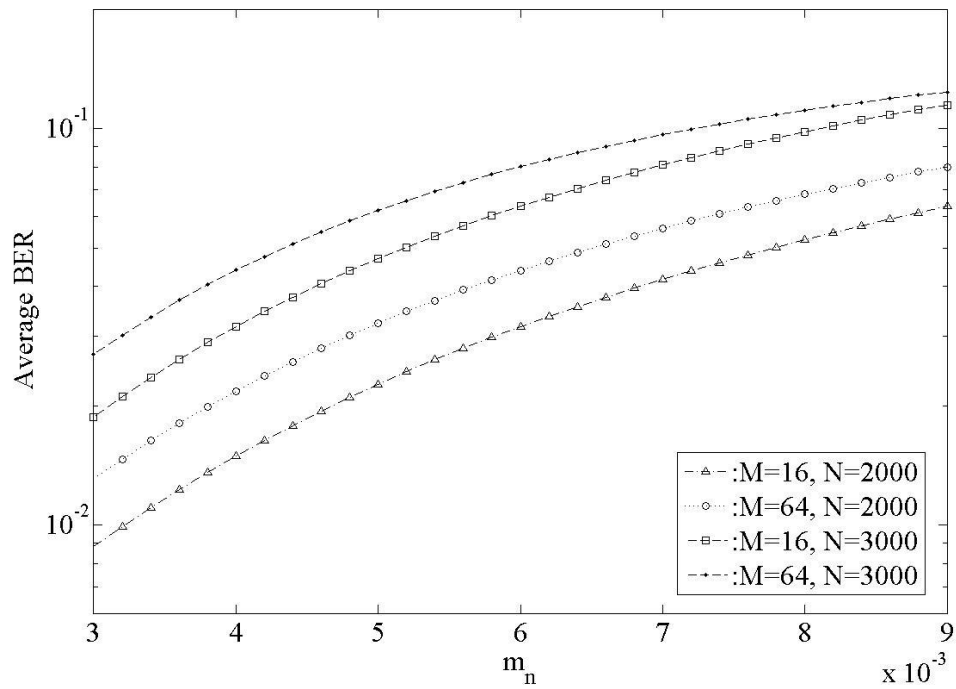
FIGURE 3. Average BER estimation for the case of atmospheric turbulence modeled with the NE distribution.
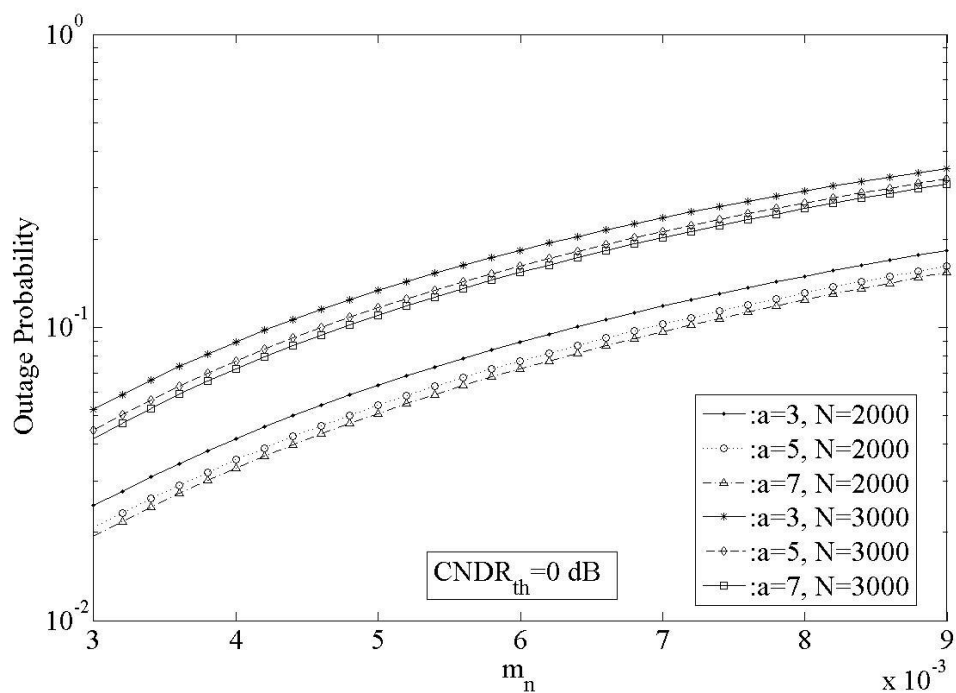

FIGURE 4. Outage Probability for the case of atmospheric turbulence modeled with the K distribution.
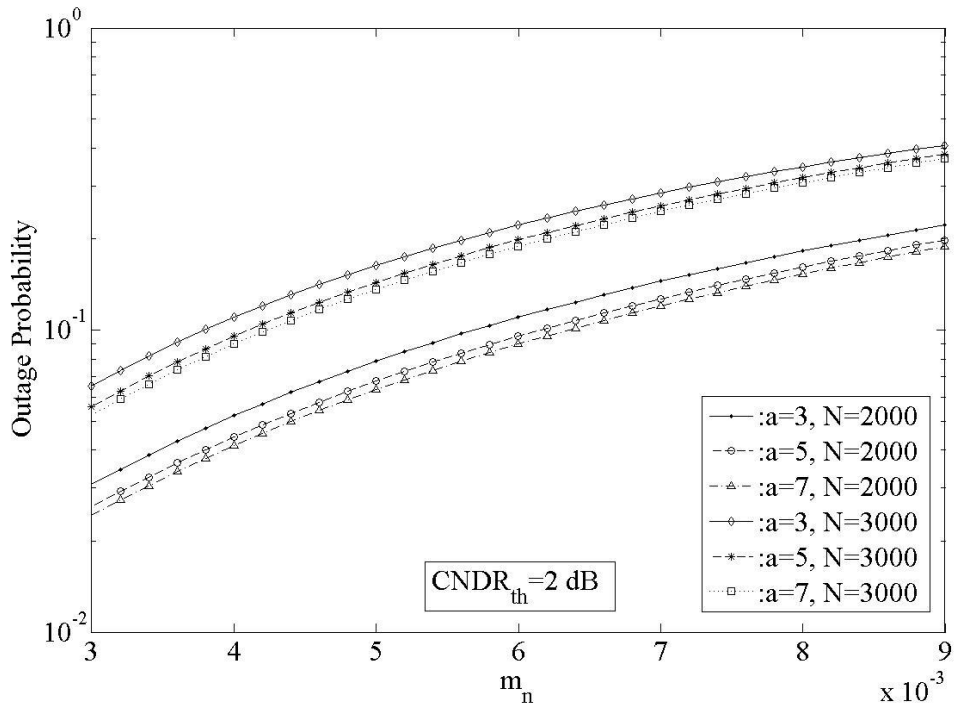
FIGURE 5. Outage Probability for the case of atmospheric turbulence modeled with the K distribution.
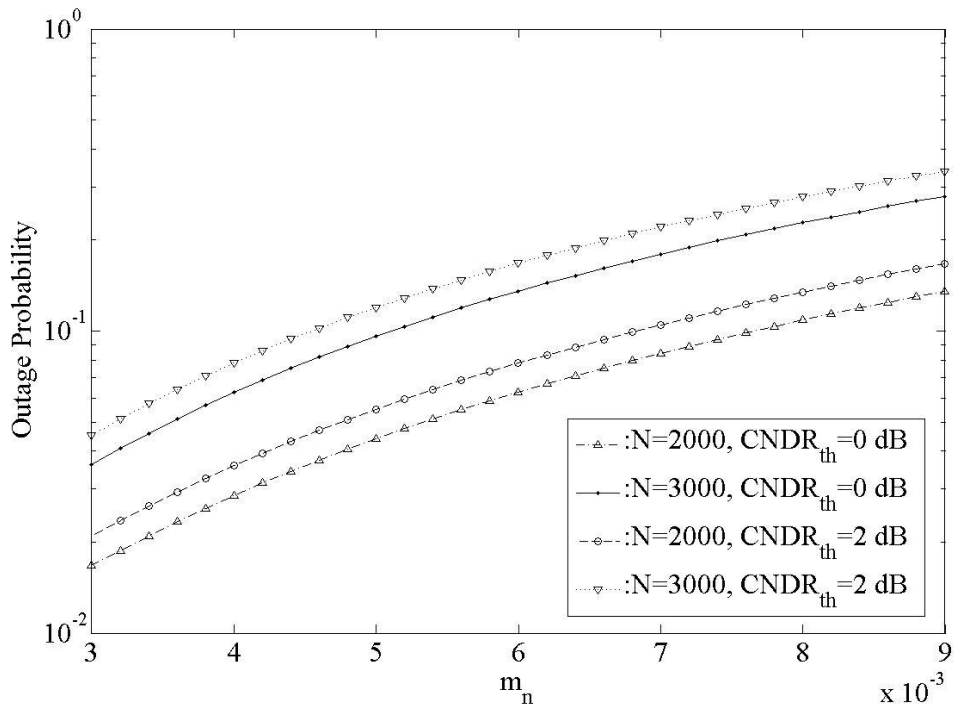

FIGURE 6. Outage Probability for the case of atmospheric turbulence modeled with the NE distribution.

VI. CONCLUSIONS

In this work we study the performance metrics of a QAM OFDM RoFSO over atmospheric turbulence channels modeled with K or the NE distribution. For this wireless optical communication system we derive closed form mathematical expressions for the estimation of the average BER and the outage probability as a function of the system's characteristics. Finally, using the derived expressions we present various numerical results for the performance of the system using common values for such communication systems.

ACKNOWLEDGMENTS

REFERENCES

1. Z. Ghassemlooy, W.O. Popoola, "Terrestrial Free-Space Optical Communications", book chapter in *Mobile and Wireless Communications: Network Layer and Circuit Level Design*, S. Ait Fares and F. Adachi (Ed.), ISBN: 978-953-307-042-1, InTech, 2010.

2. H. Henniger, O. Wilfert, An Introduction to Free Space Optical Communications, *Radioengineering*, Vol. 19, No. 2, 2010, pp. 203-212.

3. H.E. Nistazakis and G.S. Tombras, On the use of wavelength and time diversity in optical wireless communication systems over gamma–gamma turbulence channels, *Optics & Laser Technology*, Vol. 44, 2012, pp. 2088–2094, 2012.

4. G. Ntogari, T. Kamalakis and T. Sphicopoulos, Performance Analysis of Space Time Block Coding Techniques for Indoor Optical Wireless Systems, IEEE Journal on Selected Areas in Communications, Vol. 27, 2009, No. 9.

5. W.O. Popoola, Z. Ghassemlooy, E. Leitgeb, BER and Outage Probability of DPSK Subcarrier Intensity Modulated Free Space Optics in Fully Developed Speckle, *J. of Comm.*, 4, 8, 2009, pp. 546-554.

6. K. Prabu, S. Bose and D.S. Kumar, BPSK based subcarrier intensity modulated free space optical system in combined strong atmospheric turbulence, *Optics Communications*, Vol. 305, 2013, pp. 185-189.

7. V.W.S. Chan, Free-space optical communications, *J. Lightwave Technol.*, Vol. 24, No. 12, 2006, pp. 4750–4762.

8. H. Al-Raweshidy and S. Komaki, Eds., Radio Over Fiber Technologies for Mobile Communications Networks, 1st ed. Norwell, MA: Artech House, 2002.

9. A. Bekkali, C.B. Naila, K. Kazaura, K. Wakamori and M. Matsumoto, Transmission Analysis of OFDM-Based Wireless Services Over Turbulent Radio-on-FSO Links Modeled by Gamma-Gamma Distribution, *IEEE Photonics Journal*, Vol. 2, No. 3, 2010, pp. 509-520.

10. K. Kazaura, K. Wakamori, M. Matsumoto, T. Higashino, K. Tsukamoto and S. Komaki, RoFSO: A universal platform for convergence of fiber and free space optical communication networks, *IEEE Commun. Mag.*, Vol. 48, No. 2, 2010, pp. 130-137.

11. H.E. Nistazakis, A.N. Stassinakis, S. Sheikh Muhammad and G.S. Tombras, BER Estimation for Multi Hop RoFSO QAM or PSK OFDM Communication Systems Over Gamma Gamma or Exponentially Modeled Turbulence Channels, *Elsevier Optics & Laser Technology*, Vol. 64, 2014, pp. 106-112.

12. L.C. Andrews, R.L. Phillips, C.Y. Hopen, Laser Beam Scintillation with Applications, *SPIE Optical Engineering Press*, 2001.

13. H. Samimi, Coded subcarrier intensity modulated free-space optical links over generalised turbulence channels, *IET Communications*, Vol. 8, Iss. 3, 2014, pp. 335-342.

14. T. Kamalakis, T. Sphicopoulos, S.S. Muhammad and E. Leitgeb, Estimation of the power scintillation probability density function in free-space optical links by use of multicanonical Monte Carlo sampling, *Opt. Lett.*, Vol. 31, No. 21, 2006, pp. 3077–3079.

15. A. Katsis, H.E. Nistazakis, and G.S. Tombras, Bayesian and frequentist estimation of the performance of free space optical channels under weak turbulence conditions, *Journal of the Franklin Institute*, Vol. 346, 2009, pp. 315-327.

16. W. Gappmair and S.S. Muhammad, Error performance of PPM/Poisson channels in turbulent atmosphere with gamma-gamma distribution, *IET Electronics Letters*, Vol. 43, No. 16, art. no. 20070901, 2007.

17. B. Epple, Simplified Channel Model for Simulation of Free-Space Optical Communications, *IEEE/OSA J. Opt. Commun. Netw.*, Vol. 2, No. 5, 2010, pp. 293-304.

18. H.G. Sandalidis, Performance Analysis of a Laser Ground-Station-to-Satellite Link With Modulated Gamma-Distributed Irradiance Fluctuations, *J. Opt. Commun. Netw.*, Vol. 2, No. 11, 2010.

19. H.E. Nistazakis, E.A. Karagianni, A.D. Tsigopoulos, M.E. Fafalios, and G.S. Tombras, Average capacity of optical wireless communication systems over atmospheric turbulence channels, ", *IEEE/OSA Journal of Lightwave Technology*, Vol. 27, No. 8, 2009, pp. 974-979.

20. W.O. Popoola, Z. Ghassemlooy, H. Haas, E. Leitgeb and V. Ahmadi, Error performance of terrestrial free space optical links with subcarrier time diversity, *IET Communications*, Vol. 6, Iss. 5, 2012, pp. 499-506.

21. A. Jurado-Navas, J.M. Garrido Balsells, J. Francisco Paris, M. Castillo-Vasquez and A. Puerta-Notario, General analytical expressions for the bit error rate of atmospheric optical communication systems, *Optics Letters*, Vol. 36, No. 20, 2011 pp. 4095-4097.

22. H.E. Nistazakis, A Time-Diversity Scheme for Wireless Optical Links Over Exponentially Modeled Turbulence Channels, *Elsevier, Optik -International Journal for Light and Electron Optics*, Vol. 124, Iss. 13, 2013, pp. 1386-1391.

23. H.G. Sandalidis, Coded Free-Space Optical Links Over Strong Turbulence and Misalignment Fading Channels, *IEEE Transactions on Wireless Communications*, Vol. 59, No. 3, 2011, pp. 669-674.

24. H.E. Nistazakis, A.D. Tsigopoulos, M.P. Hanias, C.D. Psychogios, D. Marinos, C. Aidinis, G.S. Tombras, Estimation of Outage Capacity for Free Space Optical Links Over I-K and K Turbulent Channels, *Radioengineering*, Vol. 20, No. 2, 2011, pp. 493-498.

25. H.G. Sandalidis, T.A. Tsiftsis, Outage probability and ergodic capacity of free-space optical links over strong turbulence, *El. Lett.*, 44, 1, 2008.

26. H.E. Nistazakis, V.D. Assimakopoulos, and G.S. Tombras, Performance Estimation of Free Space Optical Links Over Negative Exponential Atmospheric Turbulence Channels, *OPTIK-International Journal for Light and Electron Optics*, Vol. 122, 2011, pp. 2191-2194.

27. A. Mostafa and S. Hranilovic, In-Field Demonstration of OFDM-Over-FSO, *IEEE Photonics Technology Letters*, Vol. 24, No. 8, 2012, pp. 709-711.

28. M. Selvi and K. Murugesan, The performance of orthogonal frequency division multiplexing in the weak turbulence regime of free space optics communication systems, *IOP Journal of Optics*, Vol. 14, art. no. 125401, 2012, 6 pages.

29. S. Dimitrov, S. Sinanovic and H. Haas, Clipping Noise in OFDM-Based Optical Wireless Communication Systems, IEEE Trans. Commun., Vol. 60, No. 4, pp. 1072-1081, 2012.

30. L. Chen, B. Krongold and J. Evans, Theoretical Characterization of Nonlinear Clipping Effects in IM/DD Optical OFDM Systems, IEEE Transactions on Communications, Vol. 60, No. 8, 2012.

31. D. Tsonev, S. Sinanovic and H. Haas, Complete Modeling of Nonlinear Distortion in OFDM-Based Optical Wireless Communication, J. Lightwave Technology, Vol. 31, No. 18, 2013, pp. 3064-3076.

32. J. Armstrong, OFDM for Optical Communications, IEEE J. Lightwave Technology, Vol. 27, No. 3, pp. 189-204, 2009.

33. J. Proakis, "Digital Communications", 4th Edition, McGraw-Hill, 2001.

34. Q. Zhang, J. Cheng and G.K. Karagiannidis, Block error rate of optical wireless communication systems over atmospheric turbulence channels, IET Communications, Vol. 8, Iss. 5, 2014, pp. 616-625.

35. V.S. Adamchik and O.I. Marichev, The Algorithm for Calculating Integrals of Hypergeometric Type Function and its Realization in Reduce System, Proc. Intl Conference on Symbolic and Algebraic Computation, pp. 212-224, Japan, 1990.

36. H.E. Nistazakis, A.N. Stassinakis, G.S. Tombras, S.S. Muhammad and A.D. Tsigopoulos, K Modeled Turbulence and Nonlinear Clipping for QAM OFDM with FSO and Fiber Serially Linked, 20th International Conference on Microwaves, Radar, and Wireless Communications MIKON-2014, IEEE Conference Proceedings, ieeexplore.ieee.org, ISBN: 978-1-4577-1435-1, DOI: 10.1109/MIKON.2014.6900015, 2014, pp. 1-4.

BER Estimation of Dual-hop PSK OFDM RoFSO Communication System over K or NE Modeled Turbulence and Optical Fiber with Nonlinear Clipping Effect

A.D. Tsigopoulos[1], M.P. Ninos[2], A.N. Stassinakis[2]

[1]*Section of Battle Systems, Naval Operations, Sea Studies, Navigation, Electronics and Telecommunications, Hellenic Naval Academy, Hadjikyriakou ave, Piraeus 18539, Greece, e-mail: atsigo@snd.edu.gr*
[2]*Dept. of Electronics, Computers, Telecommunications and Control, Faculty of Physics, National and Kapodistrian University of Athens, Athens, 15784, Greece, emails: {a-stassinakis; ninmichail}@phys.uoa.gr*

Abstract. Radio on free space optics (RoFSO) is a technology similar to the Radio over Fiber (RoF) communication systems, which enables the transmission of radio frequency signals (RF) in the optical domain through the free space. As a consequence, high capacity links are implemented with low operational and installation costs and without need of license for spectrum use. However, their performance depends strongly on the atmospheric conditions and the random changes of the propagation medium characteristics. On the other hand, using RoF links we can achieve higher bandwidths over longer distances but with the requirement of optical fiber infrastructure. In this work, we investigate the bit error rate (BER) performance metric of an optical communication system which consists of a RoFSO and a RoF link connected with a regenerator node. The orthogonal frequency division multiplexing (OFDM) technique is used in both links for the signal transmission with phase shift keying (PSK) format and the main mitigation factors which have been taken into account is the atmospheric turbulence effect, the nonlinear responsivity of the laser diode and the biasing with nonlinear clipping noise. Numerical results for realistic parameter values are derived concluding in a closed form mathematical expression for the estimation of system's BER.

Keywords: BER, OFDM, PSK, Fiber Optics, Free Space Optics, Nonlinear Clipping Effect.
PACS: 42.79.Sz, 42.81-i, 92.60.hk.

I. INTRODUCTION

Free Space Optics (FSO) and more specifically RoFSO is a very attractive and alternative solution in the absence of optical fiber links, for the interconnection of a central station to several

remote cellular base stations. The wide variety of applications of this technology is due solely to the high bit rates, the license free spectrum, the high security level and the ease of deployment. On the other hand, their efficiency depends strongly on the weather conditions such as rain, fog, snow, atmospheric turbulence etc. and the air composition like dust, smoke and other aerosol particulate matter. All these effects increase the absorption, scattering and refractive index fluctuations of the medium, degrading the received signal quality [1]-[13].

The transmission of radio signals through optical fiber cables, simply known as radio over fiber or RoF [11], facilitates the wireless access reaching higher capacity levels with significant lower signal attenuation compared to the atmospheric path. Particularly, the total losses due to the transportation of optical signal through the fiber medium is of the order of 0.2 dB/km reducing the need of relay nodes, while for the atmospheric propagation losses range from 0.2 to more than 25 dB/km depending on the weather conditions. However, optical fiber transmission requires the availability of fiber cable infrastructure and thus augmentation of the total cost, [1]-[2].

The aforementioned effect of the atmospheric turbulence is decreasing significantly the FSO link's performance and causes the well known scintillation effect which results in irradiance fluctuations at the receiver's side. Many statistical distribution models have been proposed in order to model these signal's fluctuations according to the turbulence strength. In this work, we consider the K and negative exponential (NE) distribution models which are suitable for cases with strong and saturate atmospheric turbulence conditions, respectively [14]-[17].

OFDM is a multicarrier modulation technique which offers important benefits compared to single carrier schemes such as higher spectral efficiency, robustness against frequency selective fading and elimination of co-channel and intersymbol interference. Thus, this technique, has gained popularity in many applications, like digital subscriber lines (DSL), wireless local area networks (WLAN), advanced cellular mobile networks, etc. However, the OFDM signal exhibits high peak to average power ratios (PAPR) and is very sensitive to many nonlinear effects [18]-[24].

Thus, in this work, we present a dual hop optical communication system which consists of a RoFSO segment and a RoF link connected with a decoding and forward (DF) regenerator node. The signal propagates in each link using, the PSK modulation format for each subcarrier of the OFDM scheme. The received signal in the DF node is recognized, regenerated and retransmitted by neglecting the additive noise inserted in the first part of the whole wireless optical system. So, by considering as main mitigation factors, the atmospheric turbulence and the additive distortion of the biasing and nonlinear clipping (BAC) process for the RoF segment, we conclude to a closed form mathematical expression for the estimation of the BER of the whole relayed optical wireless and fiber communication link [11], [18]-[20].

II. AVERAGE BER FOR THE WIRELESS PART OF THE OPTICAL COMMUNICATION LINK

The optical communication system under consideration consists of two segments. For the first part, we assume a terrestrial turbulent wireless optical path between the transmitter and the

DF relay node, while an optical fiber which connects the DF node with the receiver of the whole link, stands for the second part. The information transmission is carried out by using the OFDM technique which is adopted in both links. In this multiple subcarrier modulation (MSM) scheme, the initial high data rate streams are split into lower rate parallel streams which are consequently modulated into orthogonal narrowband subcarriers, each one mapped according to a modulation format. In our case, the PSK format is chosen. The OFDM signal, after the up-conversion to the carrier frequency f_c, just before the laser diode is given as [11], [19], [20]:

$$s_{OFDM}(t) = \sum_{n=0}^{N-1} s_n(t) = \sum_{n=0}^{N-1} X_n \exp\left[i\left(\omega_n + 2\pi f_c\right)t\right] \quad for\ 0 \leq t < T_s \tag{1}$$

where $\omega_n = 2\pi n/T_s$, $n=0,\ldots,$ N-1, is the angular frequency of each orthogonal subcarrier, T_s is the duration of each OFDM symbol and X_n stands for the complex data symbol of the n_{th} subcarrier coded with Gray code mapping from a 16 and 64 PSK constellation. The transmitted optical power $P(t)$ from the laser diode LD, can mathematically be expressed with the following expression, [11], [19], [20]:

$$P(t) = P_t\left[1 + \sum_{n=0}^{N-1} m_n s_n(t) + a_3\left(\sum_{n=0}^{N-1} m_n s_n(t)\right)^3\right] \tag{2}$$

where, P_t, is the average transmitted optical power, a_3 stands for the third order nonlinearity coefficient of the LD and m_n is the optical modulation index (OMI) per subcarrier, defined as $m_n = \Delta I/(I_b - I_{th})$, with ΔI being the variation of the laser driving current around a bias point and I_b, I_{th}, stand for the bias and threshold laser currents, respectively. The received optical signal at the receiver of the DF node, depends strongly on the turbulence effect after and is given through the relation $P_r(t) = P(t)L_{tot}I + n(t)$, where L_{tot} stands for the total losses caused by the atmospheric propagation, $n(t)$ is the additive white Gaussian noise (AWGN) of the channel, and I represents the instantaneous normalized irradiance at the receiver which fluctuates rapidly due to the scintillation effect caused by the atmospheric turbulence phenomenon.

The atmospheric turbulence represents a significant mitigation factor for the performance of the terrestrial wireless optical links. The random spatial and temporal refractive index variations of the propagation path, cause fluctuations of the irradiance level at the receiver and cause the so-called scintillation effect. In order to estimate these intensity fluctuations, many statistical models have been proposed based on the turbulence strength. Here, we examine the cases of strong or saturate turbulence conditions which can be modeled accurately with the K or NE distribution, respectively, [14]-[17]. Thus, the probability density function (PDF) for the normalized irradiance I of the K-distribution model is given as [14], [15]:

$$f_I(I) = \frac{2a^{\frac{a+1}{2}}}{\Gamma(a)} I^{\frac{a-1}{2}} K_{a-1}\left(2\sqrt{aI}\right) \tag{3}$$

where $\Gamma(.)$ is the gamma function, $K_x(.)$ is the modified Bessel function of the second kind and order x, α depends on the turbulence strength, i.e. larger values of α correspond to weaker turbulence and I is the normalized irradiance. Additionally, the corresponding PDF for the NE distribution is given as, [16], [17]:

$$f_I(I) = \exp(-I) \tag{4}$$

At the photo detector (PD) of the receiver at the DF relay node, the generated current is given as, [11]:

$$i(t, I) = I_0\left[1 + \sum_{n=0}^{N-1} m_n s_n(t) + a_3\left(\sum_{n=0}^{N-1} m_n s_n(t)\right)^3\right] + n_{opt}(t) \tag{5}$$

where $I_0 = \rho L_{tot} P_t I$ is the dc of the received photocurrent $i(t,I)$, ρ is the PD's responsivity, while n_{opt} is the AWGN with zero mean and variance $N_0/2$, with $N_0 = 4K_B TF/R_L + 2qI_0 + I_0^2(RIN)$. In this equation, K_B is the Boltzmann's constant, T is the temperature, F is the electronic receiver amplifier noise figure, R_L is the load resistor at the PD's side, q is the electron charge and RIN stands for the relative intensity noise from the laser. Thus, the received instantaneous carrier to noise plus distortion for each subcarrier of the OFDM, $CNDR_n$, is given accurately by the following approximate formula as, [11], [19], [20]:

$$CNDR_n(I) \approx \frac{m_n^2 \rho^2 L_{tot}^2 P_t^2 I^2}{2\left(\left[N_0/T_S\right]_{AV} + \left[\sigma_{IMD}^2\right]_{AV}\right)} \tag{6}$$

where the symbol $[.]_{AV}$ denotes the average value and σ_{IMD}^2 stands for the inter-modulation distortion (IMD), due to the nonlinear response of the LD, which affects the specific n_{th} subcarrier among N equally spaced subchannels of the OFDM scheme and depends on the third order nonlinearity coefficient, a_3, and the OMI m_n, for each OFDM subcarrier [11], [19], [20]. From (4), the expected value $[CNDR_n]_{EX}$, can be estimated, considering the expected value of the normalized irradiance, I, i.e. $E[I]$, as, [11], [19], [20]:

$$[CNDR_n]_{EX} = \frac{\left(m\rho L_{tot} P_t E[I]\right)^2}{2\left(\left[N_0/T_s\right]_{AV} + \left[\sigma_{IMD}^2\right]_{AV}\right)} \tag{7}$$

The BER of a communication system is a significant metric for the estimation of its performance. For an optical OFDM communication system which is using M-PSK modulation format the BER is given as, [19], [20], [25]:

$$P_{b,FSO} = \frac{1}{N\log_2(M)}\sum_{n=0}^{N-1}\left\{ erfc\left(\sqrt{CNDR_n(I)}\sin\left(\frac{\pi}{M}\right)\right)\right\} \tag{8}$$

where *erfc(.)* is the complementary error function and *M* is the PSK modulation format parameter.

Taking into account (8), and the PDF of the suitable distribution model, i.e. the K or the NE, the average BER for all the *N* subcarriers of the *M*-PSK OFDM RoFSO is given as [19]:

$$\left[P_{b,FSO}\right]_{AV} = \frac{1}{N\log_2(M)}\sum_{n=0}^{N-1}\int_0^\infty erfc\left(\sqrt{CNDR_n(I)}\sin\left(\frac{\pi}{M}\right)\right)f_I(I)dI \tag{9}$$

Next, by substituting in (9) the PDF of the K-distribution model, i.e. Eq. (3), we conclude to the following expression:

$$\left[P_{b,FSO}\right]_{AV,K} = \frac{2a^{\frac{a+1}{2}}}{N\Gamma(a)\log_2(M)}\sum_{n=0}^{N-1}\int_0^\infty erfc\left(\sqrt{CNDR_n(I)}\sin\left(\frac{\pi}{M}\right)\right)I^{\frac{a-1}{2}}K_{a-1}\left(2\sqrt{aI}\right)dI \tag{10}$$

while, from (9), using the PDF of the NE distribution, i.e. Eq. (4), we conclude to the following expression:

$$\left[P_{b,FSO}\right]_{AV,NE} = \frac{1}{N\log_2(M)}\sum_{n=0}^{N-1}\int_0^\infty erfc\left(\sqrt{CNDR_n(I)}\sin\left(\frac{\pi}{M}\right)\right)\exp(-I)dI \tag{11}$$

By transforming the *erfc(.)*, $K_x(.)$ and *exp(.)* functions with the corresponding Meijer functions ones, [26], the integral of (10) can be solved and we conclude to the following closed form mathematical expression for the estimation of the average BER of an M-PSK OFDM RoFSO link under strong turbulence conditions:

$$\left[P_{b,FSO}\right]_{AV,K} = \frac{N^{-1}\pi^{-\frac{3}{2}}2^{a-1}}{\Gamma(a)\log_2(M)}\sum_{n=0}^{N-1}\left\{G_{5,2}^{2,4}\left(16a^{-2}\sin^2\left(\frac{\pi}{M}\right)[CNDR_n]_{EX}\left|\begin{array}{c}\frac{1-a}{2},\frac{2-a}{2},0,0.5,1\\0,0.5\end{array}\right.\right)\right\} \tag{12}$$

where $G_{p,q}^{m,n}[\cdot]$ stands for the Meijer-function that is a standard built in function which can be evaluated with most of the well known mathematical software packages. Furthermore, this function can be transformed to the familiar hypergeometric functions, [26].

Additionally, from (12), we estimate the following closed form mathematical expression for the estimation of the average BER of an M-PSK OFDM RoFSO link under turbulence conditions modeled with the NE distribution:

$$\left[P_{b,FSO}\right]_{AV,NE} = \frac{N^{-1}\pi^{-1}}{\log_2(M)}\sum_{n=0}^{N-1}\left\{G_{3,2}^{2,2}\left(4\sin^2\left(\frac{\pi}{M}\right)[CNDR_n]_{EX}\left|\begin{array}{c}0,0.5,1\\0,0.5\end{array}\right.\right)\right\} \tag{13}$$

III. BER FOR THE OPTICAL FIBER PART OF THE COMMUNICATION LINK

In the second part of the optical communication system, between the DF node and the receiver, the signal propagates through an optical fiber. The OFDM scheme is used again with the same modulation format of M-PSK for each subcarrier. The OFDM signal, after the inverse fast Fourier transform (IFFT), is bipolar in general and cannot be applied directly to an intensity modulation/direct detection (IM/DD) system. Thus, a dc offset has to be added, in order to produce a suitable unipolar current to drive the laser diode and prevent the clipping of negative peaks. So, the instantaneous envelope of the OFDM signal is Gaussian distributed with mean μ_N and variance, σ_N^2. However, the high PAPR of the OFDM signal is a dominant disadvantage constrained by the finite linear response range for input amplitudes of the laser diode. During the biasing and clipping of the dc component after the FFT, a nonlinear clipping distortion insertion is inevitable. For such an optical OFDM communication system using M-PSK modulation format for optical fiber transmission including the BAC process, the total BER is expression (8) modified for this case as follows, [25]:

$$P_{b,OF} = \frac{1}{N\log_2(M)}\sum_{n=0}^{N-1}\left\{erfc\left(\sqrt{\gamma_{e,n}}\sin\left(\frac{\pi}{M}\right)\right)\right\} \tag{14}$$

where γ_e stands for the effective SNR given as $\gamma_e = \gamma_c\gamma_d/\left[(1+\gamma_c)(1+\gamma^2)+\gamma_d\right]$, with γ_d the SNR at the receiver, γ_c the ratio of the transmitting signal, from the regenerator node, over the nonlinear clipping noise, and $\gamma=V_{DC}/\sigma_N$ is the normalized clipping level with V_{DC} being the biasing voltage. Moreover, the value of γ_c is given as [18]:

$$\gamma_c = \left[\frac{2\gamma e^{-\gamma^2/2}}{\sqrt{2\pi}}Q(\gamma) - \frac{e^{-\gamma^2}}{2\pi} - \frac{\gamma e^{-\gamma^2/2}}{\sqrt{2\pi}} + (\gamma^2+1)Q(\gamma) - (\gamma^2+1)[Q(\gamma)]^2\right]^{-1}[1-Q(\gamma)]^2 \tag{15}$$

IV. THE TOTAL AVERAGE BER OF THE WHOLE RELAYED OPTICAL LINK

The total average BER of the whole relayed optical system can be estimated through the obtained expressions in Eqs. (12)-(15). The total BER of the whole optical communication link is estimated as, [27], [28]:

$$P_{b,Total} = P_{b,OF} + [P_{b,FSO}]_{AV} - 2P_{b,OF}[P_{b,FSO}]_{AV} \tag{16}$$

Thus, for the case of strong turbulence conditions, i.e. K-distribution model, the BER of the whole relayed optical system with M-PSK OFDM RoFSO and optical fiber link with BAC process, is given by substituting (12) and (14) in (16), and we conclude to the following closed form mathematical expression:

$$P_{b,Total,turb} = \frac{1}{N \log_2(M)} \sum_{n=0}^{N-1} \Omega + \frac{N^{-1} \pi^{-\frac{3}{2}} 2^{a-1}}{\Gamma(a) \log_2(M)} \sum_{n=0}^{N-1} \Psi_{turb} \left(1 - 2 \frac{1}{N \log_2(M)} \sum_{n=0}^{N-1} \Omega \right) \tag{17}$$

where the subscript "*turb*", stands either for the NE or K-distribution model, i.e. NE or K subscript, respectively, for the atmospheric turbulence effect,

$$\Psi_K = G_{5,2}^{2,4} \left(\frac{16[CNDR_n]_{EX}}{a^2} \sin^2\left(\frac{\pi}{M}\right) \left| \begin{matrix} \frac{1-a}{2}, \frac{2-a}{2}, 0, 0.5, 1 \\ 0, 0.5 \end{matrix} \right. \right), \Omega = erfc\left(\sqrt{\gamma_{e,n}} \sin\left(\frac{\pi}{M}\right) \right)$$

and

$$\Psi_{NE} = G_{3,2}^{2,2} \left(4 \sin^2\left(\frac{\pi}{M}\right) [CNDR_n]_{EX} \left| \begin{matrix} 0, 0.5, 1 \\ 0, 0.5 \end{matrix} \right. \right).$$

V. NUMERICAL RESULTS

In this section using expressions (12)-(14) and (17), we present the numerical results for the total average BER of the dual hop optical OFDM communication system under the K and NE turbulence, for common parameter values. The parameter value γ of the BAC process was taken equal to 6, 9 and 12 dB for optimization according to Ref. [25], while the modulation for the M-PSK format is equal to 16 and 64. The variable quantities for the estimation of the BER performance is the CNDR and SNR at the receivers of the FSO and the optical fiber link, respectively. It is obvious that these quantities can vary independently, but for simplification, here, we assume that they take the same values for both links.
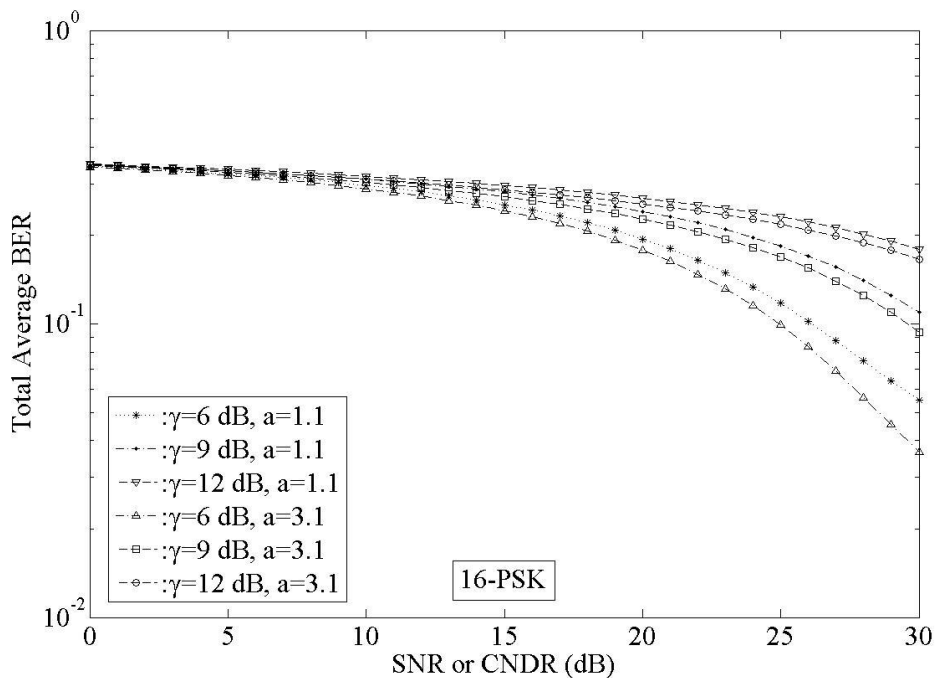

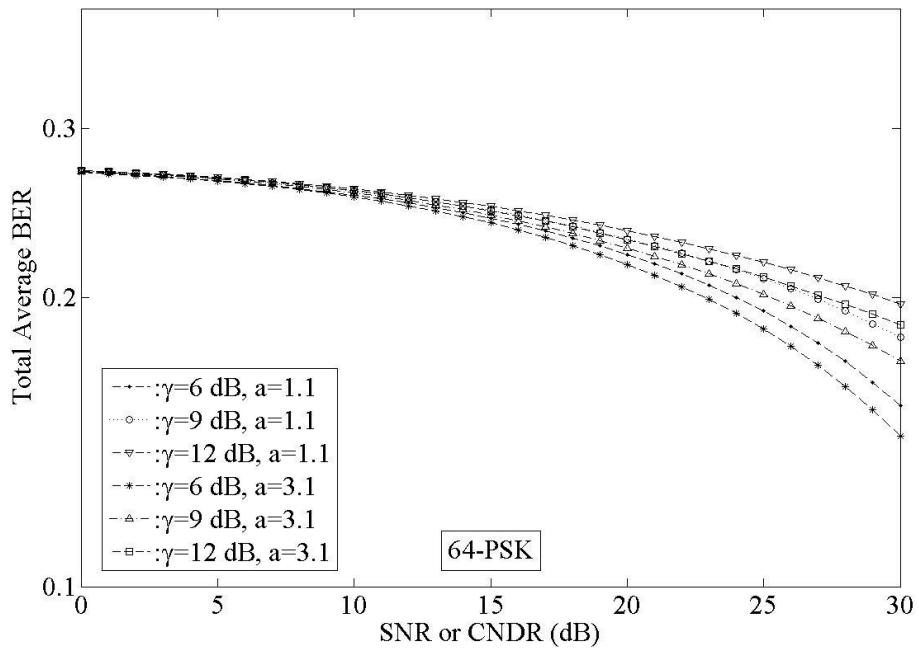**FIGURE 1.** BER estimation for the 16-PSK OFDM system with K distribution.

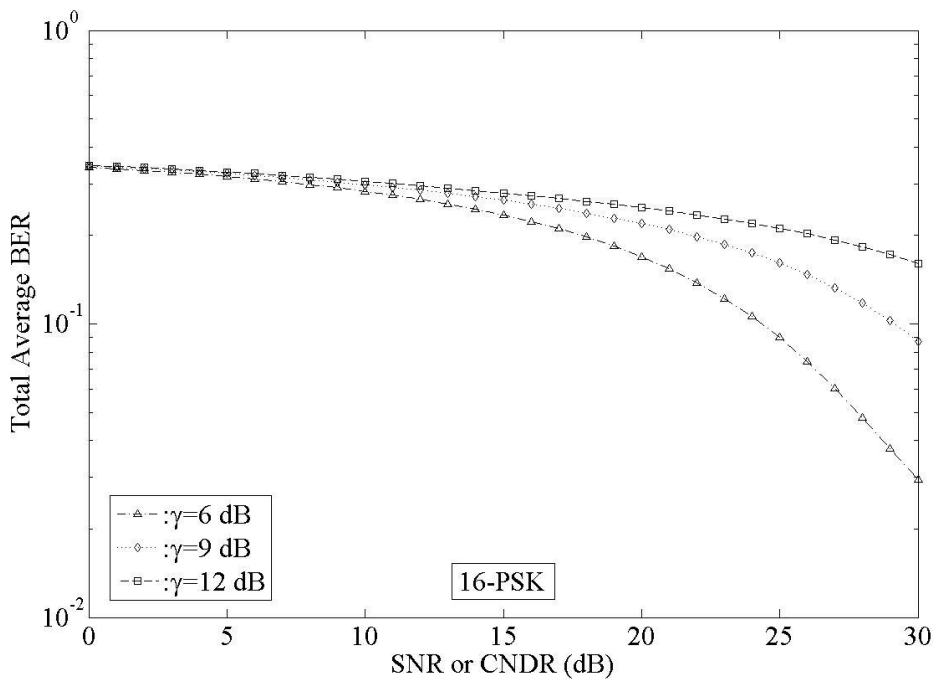**FIGURE 2.** BER estimation for the 64-PSK OFDM system with K distribution.

FIGURE 3. BER estimation for the 16-PSK OFDM system with NE distribution.
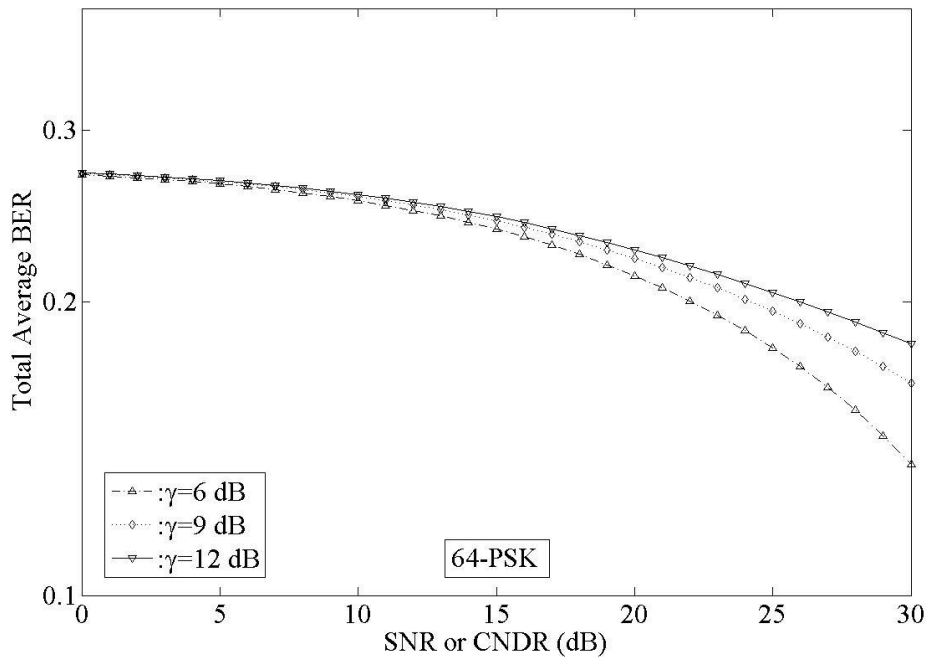
FIGURE 4. BER estimation for the 64-PSK OFDM system with NE distribution.

In Figures 1 and 2 we present the results of BER for strong turbulence conditions using the K distribution and we observe that for low SNR and CNDR values the atmospheric turbulence is the major impairment factor for the BER performance. For higher SNR and CNDR values the BAC process starting to play a significant role for the BER performance. The higher values of the BAC process parameter, conserve the BER at higher levels despite the large SNR and CNDR.

In Figures 3 and 4 we present the corresponding results for the case of saturated turbulence conditions with NE being a suitable model for such conditions. Similarly to the previous figures, we can clearly see that as parameter γ increases, the BER increases too. In all the above figures, it is also clear that for higher values of modulation format parameter M, the performance of the system becomes worse.

VI. CONCLUSIONS

In this work we studied a hybrid OFDM optical system which consists of a relayed RoFSO and RoF link which are using an M-PSK OFDM scheme. For the wireless link, we assume that the dominant performance mitigation factor is the atmospheric turbulence effect, which is modeled either with the K or NE distribution, while for the optical fiber link, the BAC process effect. For these cases we derive closed form mathematical expressions for the estimation of the average BER of each part of the optical communication link and for the whole system, as well. Finally using these expressions we present the corresponding numerical results for realistic parameter values.

VII. REFERENCES

1. Z. Ghassemlooy, W.O. Popoola, "Terrestrial Free-Space Optical Communications", book chapter in *Mobile and Wireless Communications: Network Layer and Circuit Level Design*, S. Ait Fares and F. Adachi (Ed.), ISBN: 978-953-307-042-1, InTech, 2010.

2. H. Henniger, O. Wilfert, An Introduction to Free-Space Optical Communications, *Radioengineering*, 19, 2, 2010, 203-212.

3. W.O. Popoola, Z. Ghassemlooy, E. Leitgeb, BER and Outage Probability of DPSK Subcarrier Intensity Modulated Free Space Optics in Fully Developed Speckle, *J. of Comm.*, 4, 8, 546-554, 2009.

4. D. Tsonev, S. Sinanovic and H. Haas, Complete Modeling of Nonlinear Distortion in OFDM-Based Optical Wireless Communication, *J. Lightwave Technology*, Vol. 31, No. 18, 2013, pp. 3064-3076.

5. T. Kamalakis, T. Sphicopoulos, S. S. Muhammad, and E. Leitgeb, Estimation of the power scintillation probability density function in free-space optical links by use of multicanonical Monte Carlo sampling, *Opt. Lett.*, Vol. 31, No. 21, 2006, pp. 3077–3079.

6. W. Gappmair, S. Hranilovic, E. Leitgeb, Performance of PPM on terrestrial FSO links with turbulence and pointing errors, *IEEE Commun. Lett.*, Vol. 14, No. 5, 2010, pp. 468-470.

7. H.G. Sandalidis, Coded Free-Space Optical Links Over Strong Turbulence and Misalignment Fading Channels, *IEEE Transactions on Wireless Communications*, Vol. 59, No. 3, 2011, pp. 669-674.

8. A. Katsis, H.E. Nistazakis, and G.S. Tombras, Bayesian and frequentist estimation of the performance of free space optical channels under weak turbulence conditions, *J. Franklin Inst.*, Vol. 346, 2009, pp. 315-327.

9. W. Gappmair and S.S. Muhammad, "Error performance of PPM/Poisson channels in turbulent atmosphere with gamma-gamma distribution", *IET Electronics Letters*, Vol. 43, No. 16, art. no. 20070901, 2007.

10. L.C. Andrews, R.L. Phillips, C.Y. Hopen, Laser beam scintillation with applications. *SPIE Optical Eng. Press*, Bellingham, WA 2006.

11. A. Bekkali, C.B. Naila, K. Kazaura, K. Wakamori, M. Matsumoto, Transmission Analysis of OFDM-Based Wireless Services Over Turbulent Radio-on-FSO Links Modeled by Gamma-Gamma Distribution, *IEEE Photonics Journal*, 2, 3, 2010, pp. 509-520.

12. H.E. Nistazakis and G.S. Tombras, On the use of wavelength and time diversity in optical wireless communication systems over gamma–gamma turbulence channels, *Optics & Laser Technology*, Vol. 44, 2012, pp. 2088–2094.

13. B. Epple, Simplified Channel Model for Simulation of Free-Space Optical Communications, *IEEE/OSA J. Opt. Commun. Netw.*, Vol. 2, No. 5, 2010, pp. 293-304.

14. H.E. Nistazakis, A.D. Tsigopoulos, M.P. Hanias, C.D. Psychogios, D. Marinos, C. Aidinis, G.S. Tombras, Estimation of Outage Capacity for Free Space Optical Links Over I-K and K Turbulent Channels, *Radioengineering*, Vol. 20, No. 2, 2011, pp. 493-498.

15. H.G. Sandalidis, T.A. Tsiftsis, Outage probability and ergodic capacity of free-space optical links over strong turbulence, *El. Lett.*, 44, 1, 2008.

16. H.E. Nistazakis, A Time-Diversity Scheme for Wireless Optical Links Over Exponentially Modeled Turbulence Channels, *Elsevier, Optik -International Journal for Light and Electron Optics*, Vol. 124, Iss. 13, 2013, pp. 1386-1391.

17. H.E. Nistazakis, V.D. Assimakopoulos, and G.S. Tombras, Performance Estimation of Free Space Optical Links Over Negative Exponential Atmospheric Turbulence Channels, *OPTIK-International Journal for Light and Electron Optics*, Vol. 122, 2011 pp. 2191-2194.

18. L. Chen, B. Krongold and J. Evans, Theoretical Characterization of Nonlinear Clipping Effects in IM/DD Optical OFDM Systems, *IEEE Transactions on Communications*, Vol. 60, 2012, No. 8.

19. H.E. Nistazakis, A.N. Stassinakis, S.S. Muhammad and G.S. Tombras, BER Estimation for Multi Hop RoFSO QAM or PSK OFDM Communication Systems Over Gamma Gamma or Exponentially Modeled Turbulence Channels, *Elsevier Optics & Laser Technology*, Vol. 64, 2014, pp. 106-112.

20. H.E. Nistazakis, A.N. Stassinakis, H.G. Sandalidis and G.S. Tombras, "QAM and PSK OFDM RoFSO over *M*-Turbulence Induced Fading Channels", *IEEE Photonics Journal*, Vol. 7, No. 1, DOI: 10.1109/JPHOT.2014.2381670, 2015.

21. Q. Shi, Asymptotic Clipping Noise Distribution and its Impact on M-ary QAM Transmission Over Optical Fiber, *IEEE Trans. Commun.*, 43, 1995, pp. 2077-2084.

22. A. Mostafa and S. Hranilovic, In-Field Demonstration of OFDM-Over-FSO, *IEEE Photonics Technology Letters*, 24, 8, 2012, pp. 709-711.

23. S. Dimitrov, S. Sinanovic and H. Hass, Clipping Noise in OFDM-Based Optical Wireless Communication Systems, *IEEE Trans. Commun.*, Vol. 60, No. 4, 2012, pp. 1072-1081.

24. A.J. Lowery, L.B. Du and J. Armstrong, Performance of Optical OFDM in Ultralong-haul WDM Lightwave Systems, *IEEE J. Lightwave Technology*, Vol. 25, No. 1, pp. 131-138, 2007.

25. J. Proakis, Digital Communications, 4th Edition, *McGraw-Hill*, 2001.

26. V.S. Adamchik and O.I. Marichev, The Algorithm for Calculating Integrals of Hypergeometric Type Function and its Realization in Reduce System, Proc. Intl Conference on Symbolic and Algebraic Computation, Japan, 1990, pp. 212-224.

27. E. Morgado, I. Mora-Jiménez, J. J. Vinagre, J. Ramos and A.J. Caamaño, End-to-End Average BER in Multihop Wireless Networks over Fading Channels, *IEEE Transactions on Wireless Communications*, Vo. 9, 2010, No. 8.

28. H.E. Nistazakis, A.N. Stassinakis, G.S. Tombras, S.S. Muhammad and A.D. Tsigopoulos, *K Modeled Turbulence and Nonlinear Clipping for QAM OFDM with FSO and Fiber Serially Linked*, *20th International Conference on Microwaves, Radar, and Wireless Communications MIKON-2014*, *IEEE Conference Proceedings*, *ieeexplore.ieee.org*, ISBN: 978-1-4577-1435-1, DOI: 10.1109/MIKON.2014.6900015, 2014, pp. 1-4.

Atmospheric Effects on EM Propagation and Weather Effects on the Performance of a Dual Band Antenna for WLAN Communications

E.A. Karagianni, A.P. Mitropoulos, I.T. Latif, A.G. Kavousanos-Kavousanakis, J.A. Koukos and M.E. Fafalios

Hellenic Naval Academy, Department of Naval Sciences, Section of Battle Systems, Naval Operations, Sea Studies, Navigation, Electronics and Telecommunications, Hatzikyriakou Ave., Piraeus, 18539, Greece, e-mails: {evka;akavousa;koukos;fafalios}@hna.gr

Abstract. Despite the fact that most of the research studies are based on "free space electromagnetic waves analysis", this consideration is only an approximation. In order to accurately predict an antenna performance, we must include the effects of the earth and its atmosphere in EM (electromagnetic) waves' propagation. This should account for ground reflections, diffraction, bending or refraction of EM waves and attenuation or absorption of EM energy by the small particles constituting the atmosphere. More specifically, in radar systems the unwanted returns are referred to as clutter. These returns may be from the surface, surrounding the target (ground), or from the volume of space around it (rainfall). In this paper, precipitation effects on the EM wave propagation are presented. Moreover, the rapid development in the field of Wireless Local Area Networks (WLANs) demands the existence of devices capable of operating in more than one frequency bands. For this reason the design of a printed antenna to conform to multiple communications protocols, in the band of 2.4GHz and 5.1GHz, is presented in this paper. A microstrip-fed printed bow-tie antenna is designed and simulated in order to achieve dual bandwidth, high gain, and size reduction. The patch antenna is designed with the help of the High Frequency Structure Simulator and the design optimization is based on the variation of its shape, the conductive material, the nature and the thickness of the substrate, in order to have a structure which resonates in the frequencies used for Wi-Fi applications. Simulation results confirm a strong dependence of propagation losses on the humidity of the atmosphere.

Keywords: Wireless Local Area Networks; Microstrip Antennas; Weather Phenomena; Precipitation; Relative permittivity; Refractivity.
PACS: 41.20.Jb; 42.25.Dd; 42.25.Fx; 42.68.Ay; 42.68.Bz; 42.68.Ge; 92.60.Jq; 92.60.Ta ; 42.25.Bs; 77.22.-d; 84.30.-r; 84.40.Dc.

I. INTRODUCTION

One of the main goals of every individual or organized society is the provision of adequate telecommunications links, especially on wireless internet. Therefore, many hotel units, ports or

commercial enterprises advertise free Wi-Fi throughout their own area, while all organized companies provide Wi-Fi access, even with restrictions on access (passwords, limited data quantity or quality on accessible information). The USA President himself, has set a goal to reach 98% of all Americans to be able to access to wireless internet, with the hope of bringing every part of America into the digital age by 2016 [1].

The rapid advances in the wireless communication industry demand novel antenna designs that could be used in more than one frequency bands and that will allow size reduction [2]-[4]. Therefore, the design of small antennas suitable for portable devices covering multiple bands such as GSM900, DCS1800, PCS1900, UMTS2000, ISM2450, is of great interest. Many techniques have been proposed for the design of radiating elements of this type, the great majority of which are microstrip antennas. The common feature is that they usually come from an ordinary shape which is perturbed in appropriate schemes [5], [6].

Furthermore, one of the major criteria to the antenna design is the low profile. People do not want to see a large hideous metal mounted near a historical building which could ruin the scenery. It must be relatively small and fit in almost any space. The antenna has to be of low weight, so it can be easily mounted without the need of heavy mechanisms which could cause an ugly landscape and an increase in cost.

The design of a multi-frequency band printed antenna is a difficult task and in many cases is an art [7], [8]. It requires that the efficient operational characteristics must be ensured in all the frequency bands of operation, such as Gain greater than 0dB and small reflection coefficient at the feeding port. Furthermore, these properties must not be obtained at the cost of a complex feeding network, a non compact fabrication or an antenna arrangement of large size [9], [10]. Therefore the design of this type of antennas is a difficult task and any novel concept or modification of the existing methods is useful.

II. ANTENNAS FOR WLAN COMMUNICATIONS

2.1. Bands for IEEE802.11

The motivation for this work is the high cost of designing and maintaining acoustic and optical systems. WLAN has the potential to provide an ideal solution for certain applications, where high data rate transmission is required at short distances. Because WLAN devices are globally available, their cost is relatively low and there is adequate knowledge in handling them. Also, due to the fact that WLAN can operate in frequency spectrums that have been released for free public use like unlicensed ISM (Industrial, Scientific and Medicine) radio bands, there is no cost for using these frequencies. In spite of the real purpose of the ISM bands, there has been a rapid growth in their use in low-power, short-range communications platforms.

IEEE 802.11 is the current standard for WLAN. Most people refer to WLAN as Wi-Fi. It has four popular protocols: 802.11a, 802.11b, 802.11g, and 802.11n. While 802.11a operates at 5 GHz, 802.11b and 802.11g operate at the 2.4GHz. Furthermore, 802.11n operates at both 2.4 GHz and 5GHz band. Nowadays, 802.11ac is becoming more popular among vendors.

The 2.4 GHz band is divided up into fourteen channels which have a bandwidth of 22 MHz for 802.11b and 20MHz for 802.11g and is more popularly used than the 5 GHz band. This means that there are many users in these frequency ranges including wireless phones, microwave ovens or even baby monitors, which amend to the rising of the ambient noise and interference and thus making communication less effective. Due to the fact that from those fourteen channels, only three of them (1, 6 and 11 with center frequencies of 2412, 2437 and 2462 MHz respectively) do not overlap with each other and that all other channels overlap with each other and with the aforementioned three channels, a safe conclusion can be made that there is a strict

limitation in the quantity of the concurrently existing non interfering Access Points (AP). Channel 14 also does not overlap with channel 11, but the lack of separation between these channels might create many problems. According to 17.4.6.3 Channel Numbering of operating channels [11], "In a multiple cell network topology, overlapping and/or adjacent cells using different channels can operate simultaneously without interference if the distance between the center frequencies is at least 25 MHz". For this reason exactly, even though channels 1, 5, 9 and 13 seem to non overlap when used for 802.11g communications, the concurrent usage of them is avoided but under no circumstances prohibited. Finally, there are many countries that do not allow the full usage of the spectrum such as Central and North American countries which for instance allow the usage of channels 1 through 11 and thus limiting more their availability.

On the other hand, the 5 GHz band operates between the frequencies of 5.1 to 5.8 GHz with wider channel-widths up to 80 or even 160 MHz (802.11ac). The number of distinct none overlapping channels is up to twenty one, which provides the availability of using a greater amount of concurrent non interfering APs.

The 2.4 GHz has long been a standard around the world, while the usage of many channels within the 5 GHz band is prohibited in some countries, like China. One reason to use the lower frequency band is because the waves of the 2.4 GHz band have a better propagation behavior through obstacles than that of the 5 GHz band waves and thus provides better coverage. On the other hand, the main reason to use the 5 GHz band is that it is not used as widely as the 2.4 GHz band so there is less interference from neighboring Wi-Fi signals. Also, the higher the frequency is kept, the smaller the size of the antenna should be, meaning that 5 GHz waves need cheaper (in general terms) antennas which can be designed and built easier.

TABLE [1]. Various Wireless Standards

Standard	Frequency	Data Rate
IEEE 802.11b	2.4 GHz	11 Mbps
IEEE 802.11g	2.4 GHz	54 Kbps
IEEE 802.15.4	2.45 GHz (Worldwide)	250 Kbps
IEEE 802.15.4	868/915 MHz (N. America/Europe)	20/40/100 Kbps
IEEE 802.11a	5 GHz	54 Kbps
IEEE 802.11n	2.4/5 GHz	54 Kbps – 600 Mbps
IEEE 802.11ac	5 GHz	1300 Mbps

IEEE 802.15.4 standard supports communications up to 10 meters in free space propagation. Different atmospheric phenomena such as heavy rain or snowfall or even high humidity are expected to reduce more the effective range of the propagation and the quality of communication, more when operated in the 2.4 GHz frequency than operated the 868 or 915 MHz. Mainly this type of communication has been designed for very low-power consumption applications and enjoys strong interest, since consumption is a key factor in deployable sensor infrastructures.

2.2. Highly Directive Antennas

A highly directive antenna allows the signal from the WLAN Access Point (AP) to be aimed at a designed location. Signal can be directed towards high density location and provide WLAN to users. This provides a convenient way to provide an extended coverage area for a high density of people area, without the need of installing more APs. The same antenna would be beneficial in ships. A directional antenna can provide internet access to other ships in the same neighborhood.

Radiation efficiency E, is the "ratio of the total power radiated by an antenna to the net power accepted by the antenna from the connected transmitter" [12]. In the best case scenario, the maximum power accepted by the transmitting antenna is 50% of the total power supplied and this occurs when the generator impedance and the antenna are matched, usually to 50Ω. In practice, the radiation resistance has to be big and the loss resistance has to be as small as possible. The efficiency of an antenna is given by

$$E = \frac{P_{rad}}{P_{in}} = \frac{R_R \cdot I^2}{(R_R + R_L) \cdot I^2} = \frac{1}{1 + \frac{R_L}{R_R}} \tag{1}$$

where R_L is the loss resistance which corresponds to the loss of the antenna, R_R is the radiation resistance, P_{rad} is the power radiated by the antenna and P_{in} is the power input to the antenna.

Directivity D in a particular direction is "the ratio of the power density radiated in that direction to the power density that would be radiated in that direction if the antenna were an isotropic radiator (radiates equally in all directions).

This is similar to that of antenna gain with the following difference: the antenna gain takes into account the efficiency of the antenna whereas directivity takes into account the losses gain. Directivity can be calculated using the Poynting Vector P (energy flux in W/m^2), which gives the average real power per unit area radiated by an antenna in free space [13]. The equation for the directivity of an antenna is given by

$$D = \frac{P}{P_0} = \frac{P \cdot 4 \cdot \pi \cdot r^2}{P_{rad}} \tag{2}$$

where P_{rad} is the total power radiated by the antenna, P is the power density at distance r and $P_0 = \frac{P_{rad}}{4 \cdot \pi \cdot r^2}$ [14].

The antenna gain takes into account losses, so the gain of an antenna will always be less than the directivity. Knowing the directivity of the antenna, the total power radiated by the antenna, and the received power which takes into account loss, the antenna gain is

$$G = D \cdot E \leq D \tag{3}$$

2.3. Antenna Arrays

An antenna array is "an antenna comprised of a number of identical radiating elements in a regular arrangement and excited to obtain a prescribed radiation pattern" [15], [16]. Antenna arrays can be divided into two categories: Scanning and non-scanning antenna arrays. Scanning arrays are able to move their main beam electronically, usually by changing the phase of the elements. Non-scanning array can only change their main beam lobe by moving the antenna orientation and they are usually used for directional radiation applications. A common type of scanning array is the phased array. Non-scanning array examples are an array of dipoles, or a microstrip antenna. The multiple radiating elements of phased array antennas are connecting to a phase shifter. The phase shifting allows the radiation pattern to be "steered" towards a certain direction.

2.4. Antenna's Type Selection

Different antenna configurations were studied. Various types of high gain antennas were compiled to be considered for the WLAN possible antenna design. All types can provide sufficient gain with the use of a plain, parabolic, or corner reflector [14].

Aperture antennas use a waveguide and branch into an aperture which can be designed to achieve a desired high gain. They may be expensive depending on the type of the material used. Phased array radiation pattern can be changed by varying the phase of each/or certain radiating element. It can provide high gain but it can also be configured to direct high gain signals to multiple users in various directions.

Helix antenna in axial mode can produce directive radiation patterns. Axial mode helix antennas can be mounted easily, but the helix structure extends into the horizontal plane. The structure may not withstand high speed wind and may face problems in colder weather. Depending on how many turns(helices) are needed to achieve the desired gain, the antenna can be extremely long and may require a stronger middle support. Phased array antennas are expensive to manufacture with the cost increasing along with the number of the radiating elements. Phase shifters, numerous feeds, and multiple cables are needed. In addition, the building and assembling of a phased array requirew more time than any other antenna configuration.

Dimensions of a horn antenna are more complicated and one may be hard to manufacture. Last, but not least, reflector antennas cannot be considered as low profile antennas, especially parabolic reflectors. In addition, the reflectors are made of metal and are much heavier than a microstrip or a helix antenna.

Microstrip antennas can provide directivity in the range of 7 to 9 dBi. An array of microstrip antennas can achieve a considerable higher gain. These antennas have a smaller cross-sectional area than the reflector antennas achieving the same gain, and are overall smaller than the parabolic antennas. Microstrip antennas are also low profile and can be mounted with simple screws. In addition, they can be designed to be completely weather proof. The cost of manufacturing a microstrip antenna can be inexpensive using cheap substrate material and thin conductive foil. For the same reason they are of light weight [17], [18]. A microstrip antenna is selected for this application.

III. ATMOSPHERIC EFFECTS ON EM WAVES

3.1. Troposphere Layer and EM waves

The troposphere layer extends from the Earth surface up to approximately 20 km above it and includes climatic phenomena such as rain, snow, cloud, fog, wind, and storms. Electromagnetic waves passing through the Earth atmosphere are subjected to the following major effects: Absorption and attenuation, reflection, refraction, changes of polarization, scattering and diffusion.

The velocity v of EM waves is related to the light velocity in free space c and to the relative permittivity ε_r and permeability μ_r of the medium [7].

In linear media, the frequency does not change when the EM wave goes from one medium to another. The velocity of an EM wave propagating at every frequency in distilled-water where μ_r=1 and ε_r=81 is $v \approx 0.3 \cdot 10^8 \frac{m}{s}$. Since we assume that the medium characteristics are constant with frequency, propagation velocity does not depend on the frequency, thus for every

frequency the velocity is the same, but the wavelength (λ) differs. However, one of main features of wet particles like rain, snow, etc, is their frequency-dependent attenuation. The index of relative permittivity can be introduced as follows

$$\varepsilon_r = \varepsilon_r' - j \cdot \varepsilon_r'' \tag{4}$$

where ε'_r is the real part of relative permittivity index and causes reflection and scattering of waves, while ε''_r is its imaginary part which introduces absorption of wave power and eventually imposes attenuation on it.

The relative permittivity of the air depends on the temperature T in ^{0}K, the localized atmospheric pressure P in mbars and the water vapor pressure e in mbars too [19]-[21].

$$\varepsilon_r = 1 + 155.1 \cdot 10^{-6} \cdot \frac{P}{T} + 746 \cdot 10^{-3} \cdot \frac{e}{T^2} \tag{5}$$

EM waves passing through a lossy medium will be attenuated. The depth of penetration (δ) is defined as a distance in the medium at which the wave amplitude of an EM wave incident at surface falls to 1/e of its initial value. In a conductor or medium with good conductivity, the depth of penetration denoted by δ is inversely proportional to the square root of the frequency, so it reduces while increasing frequency. By simple calculations it may be verified that for frequencies of more than 100 KHz, propagation of EM waves in Earth land and sea-water is lossy. Even for VLF bands the wave is descending remarkably in long distances.

3.2. Refraction and Spherical Scatterers

When an EM wave propagates through a medium which consists of atoms and molecules, it will interact with that medium through various processes, two of them being absorption and scattering. The efficiency of the interaction is related to the amount of signal absorption. Changes in propagation velocity due to this interaction result in a change in the wave's direction, called refraction and is described by the index of refraction n. Water, similarly to air has non magnetic properties, thus μ_r=1 and the index of refraction, is

$$n = \sqrt{\varepsilon_r} \tag{6}$$

Using equations (5) and (6) and selecting the first three terms of the binomial expansion, it yields that

$$n = 1 + 77.6 \cdot 10^{-6} \left(\frac{P}{T} \right) - 5.6 \cdot 10^{-6} \cdot \left(\frac{e}{T} \right) + 3.73 \cdot 10^{-1} \left(\frac{e}{T^2} \right) \tag{7}$$

where n is the index of refraction, T is the temperature in ^{0}K, P is the localized atmospheric pressure in mbars and e is the water vapor pressure in mbars.

To alleviate the use of exceedingly small numbers, another parameter definition is introduced, called refractivity (N) and is related to n by

$$N = (n-1) \cdot 10^6 = 77.6 \cdot \left(\frac{P}{T} \right) - 5.6 \cdot \left(\frac{e}{T} \right) + 3.73 \cdot 10^5 \left(\frac{e}{T^2} \right) \tag{8}$$

There is a strong variability due to humidity (vapor pressure). On average, refractivity decreases with altitude, but at a gradually decreasing rate [8]. Also, a new parameter called modified refractive index and denoted by n_M is defined by

$$n_M = n + \frac{h}{R_e} \qquad (9)$$

where n is the refractive index of the air, h is the height of the location (altitude) and R_e is the Earth radius. The last two parameters have the same unit.

There is another parameter called refractive modulus or modified refractivity and is defined according to the following equation

$$M = (n_M - 1) \cdot 10^6 = N + 10^6 \cdot \frac{h}{R_e} \qquad (10)$$

It is important to summarize that only minor changes in refractive index are necessary to cause a significant change in energy propagation. By using the relationship between refractivity N and refractive index, n can be derived in terms of total pressure, temperature, and water vapor concentration, as shown in Equation (7). Variations of temperature and moisture in the propagation path cause local refraction of the signal, resulting in signal loss and increase of noise [19].

It is often more convenient to represent EM radiation as rays of energy instead of waves. Rays are lines along which waves travel and are drawn perpendicular to each wave front. Snell law is a formula used to describe the relationship between the angles of incidence and refraction, of rays passing through a boundary between two different isotropic media:

$$n_1 \cdot \sin\theta_1 = n_2 \cdot \sin\theta_2 \qquad (11)$$

where θ_1, θ_2 are the incoming and outgoing incident angles respectively, and n_1, n_2 are the materials.

These values are used to represent the factor by which a wave's speed decreases when traveling through a refractive medium. Snell law quantifies these speed changes in the form of angular change, rather than the degree of "bending" of the ray. This bending is one key factor which affects the propagated signal strength. Additionally, by knowing the refractive index in the atmosphere at each level, one can predict the path that the EM waves will follow.

Scattering of EM radiation plays a significant part in the total of atmospheric effects. Scattering is a function of several factors: particle shape, size, index of refraction, wavelength (λ) and geometry. In 1908 Mie applied Maxwell's equations (which describe EM radiation) to the case of a plane electromagnetic wave incident on a sphere. Mie showed that for a spherical scatterer, the scattered radiation is a function of only viewing angle, θ, and the size parameter χ, defined as:

$$\chi = \frac{2 \cdot \pi \cdot r}{\lambda} \qquad (12)$$

This size parameter can be used to divide scattering into three regimes. Mie scattering occurs for size parameters in the range of values between 0.1 and 50, in which the wavelength of the radiation and the periphery of the particle are comparable. Rays undergoing Mie scattering are strongly scattered forward and backward. The second regime is for size

parameter values greater than approximately 50. The scatterer is large in comparison to the wavelength of the radiation and results in Geometric optics, widely observed in the occurrence of rainbows following a storm. Finally, Rayleigh scattering results when the size parameter is much smaller than the given wavelength and thus is largely insensitive to particle shape [22].

3.3. Discussion on Propagation Phenomena

EM wave refraction in the Earth atmosphere has several effects on the wave propagation and can result in transition of the wave over the horizon. It can be assigned to a straight line for propagation path of waves, provided that a new equivalent radius R'_e is assumed for the Earth instead of the real Earth radius R_e. For standard atmosphere, calculations resulted in $R'_e = 8500$ km while actual radius of the Earth is $R'_e = 6371$ km.

The Earth atmosphere is more diluted as the height increases, thus the index of refraction is reduced. Variation of the refraction index is usually continuous and it causes to smooth the wave curvature. In case of assuming a direct path for EM wave propagation, denoted by R, the K-factor is defined as the ratio of equivalent radius of the Earth R'_e to its actual value R_e as in the following equation

$$K = \frac{R'_e}{R_e} = \frac{R}{R - R_e} \tag{13}$$

K-factor is about 1.33 for the standard conditions (EM waves path R=25000 km), based on equation (17). Due to some natural phenomena, the equivalent Earth radius is reduced and sometimes is less than real Earth radius. This situation, which is equivalent to K-factor value being less than 1, causes high bulge on Earth surface and produces an obstacle to the EM waves' propagation near the Earth surface [19].

Refractive losses, specifically those due to changes in wave propagation speed through a medium, can result in changes of the signal amplitude. Constructive interference results in an increase of the amplitude, while destructive interference can reduce the amplitude of the received signal. These effects are due to multipath, which is the propagation phenomenon resulting when an EM wave reaches the receiving antenna from two or more paths. Causes of multipath include atmospheric ducting, ionospheric reflection and refraction, and reflection from terrestrial objects, such as mountains, buildings or ocean waves. Additionally, the influence of multipath depends on frequency, path length and the reflection coefficient of the surface [22]-[33].

Modified refractivity is used to determine how rays are bent relative to the Earth's curvature and assist in determining regions of ducting. Thus, ducts, which can be surface based or elevated, are simply atmospheric layers that have formed when M decreases with height. Radar or other EM waves can be "trapped" within and may result in greater energy propagation than normally expected [26]-[35].

In addition to ducting, EM waves can also be refracted in different ways and their behavior forms the basis of the classes of refractivity. When rays are sub-refracted, their propagation distance to the horizon decreases.This occurs when dM/dh is greater than 157. Conversely, super-refracted rays occur when dM/dh varies between 0 and 78. A an effect the distance of the propagation will increase. Finally, normal refracted rays occur for dM/dh between 78 and 157. In such casethe distance of propagation seems to be unaffected.

Equation (15) takes into account only air gases and does not consider liquid water content or free electron density. The presence of liquid water usually has negligible effect on N for the

band of frequencies of interest. The presence of free electron density is important only for high atmospheric attitudes, typically above 60 km.
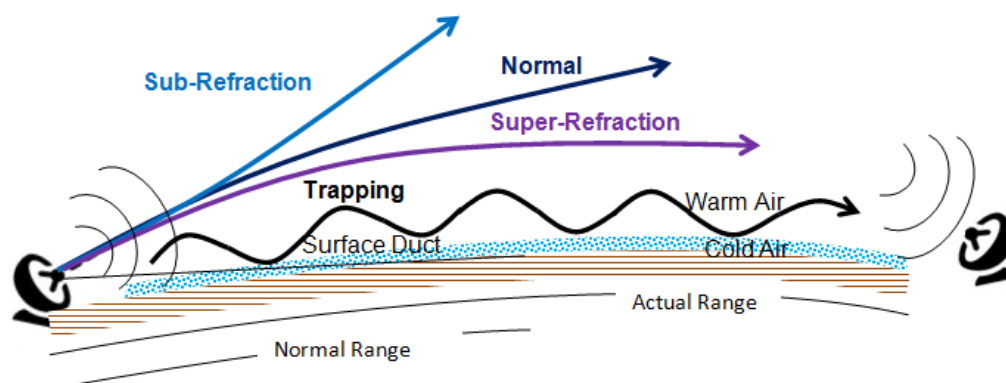

FIGURE 1. Propagation paths for various atmospheric reflective index conditions.

3.4. Earth Effects above the Seawater

The Earth effects consist of the following main factors [19], [26], [35]: Mountains and hills, forests, woodlands, vegetation covers, oceans, seawater, rivers, flat and coastal areas. VHF and UHF EM propagation above the seawater has the following main points:
- The sea surface is a good reflector for EM waves. In some conditions, detected signals in the receiver are the summation of propagated and reflected waves.
- The sea water attenuation index is very big and the penetration depth is very small.
- Cold and warm water have different effects on EM waves propagation. One of the most important effects of seawater in EM propagation is the creation of an air duct which is more significant in warm zones due to the settlement of water vapors (figure 1).
- The obstacle in EM wave's propagation is only high sea-waves which can be created from strong storms.

3.5. Weather Effects in the upper UHF band propagation

When EM waves propagate in atmosphere, are affected by magnetic storms, sky noise, sun spots, and also atmospheric events like rain, cloud, snow, hail, fog, humidity, wind or terrestrial parameters like mountains, forests, and seas.

Some important climate factors and their possible effects to the upper UHF band wireless communications are:
- Atmospheric particles like Oxygen, Nitrogen, and other natural gases may not affect the EM wave propagation due to their low χ factor.
- Water vapor, fog, and air dust of comparable dimensions compared to the wavelength of UHF band, affect wave propagation.
- Wind produced by the motion of atmospheric molecules, has positive effects on wave propagation.
- Atmospheric precipitations such as rainfall, snow, and hail do not have tangible effects on amplitude attenuation and reflection in VHF band wave propagation but their effect is becoming important in 2.4 GHz and 5.1GHz.

- Air index of refraction variations will cause K-factor variations. In general, the normal values of K in VHF and UHF communications are: In VHF band it is similar to standard condition (equal to 1.33). In lower UHF band (less than 1GHz), K-factor is normally about 1–1.33. In upper UHF band, consisting of frequencies between 1 and 3GHz, K-factor is normally about 1 with 25% tolerance.
- Earth magnetic field effects which may cause the rotation of EM waves in elevated layers are negligible on the upper UHF band.
- Galaxy, sky, and sun noises are small as the frequency increases.

3.6. Attenuation due to Rain Rate

The specific attenuation γ_R (dB/km) is obtained from the rain rate R (mm/h) using the power-law relationship [39]:

$$\gamma_R = kR^\alpha \tag{14}$$

Values for the coefficients k and α are determined as functions of frequency, f (GHz), in the range from 1GHz to 1 THz, from the following equations, which have been developed from curve-fitting to power-law coefficients derived from scattering calculations:

$$\log_{10} k = \sum_{j=1}^{4} a_j \exp\left[-\left(\frac{\log_{10} f - b_j}{c_j}\right)^2\right] + m_k \log_{10} f + c_k \tag{15}$$

and

$$\alpha = \sum_{j=1}^{5} a_j \exp\left[-\left(\frac{\log_{10} f - b_j}{c_j}\right)^2\right] + m_\alpha \log_{10} f + c_\alpha \tag{16}$$

where f is the frequency in GHz, m_k=-0.18961, c_k=0.71147, m_a=-0.05374, c_a=0.83433 and the values for the constants a_j, b_j and c_j are given in table [2]

	TABLE [2].		
J	a_j	b_j	c_j
1	-5.3398	-0.1001	1.1310
2	-0.3535	1.2697	0.4540
3	-0.2379	0.8604	0.1535
4	-0.9416	0.6455	0.1682

For linear and circular polarization, and for all path geometries, the coefficients in equation (19) can be calculated using the following equations:

$$k = \frac{k_H + k_V + (k_H - k_V)\cos^2\theta \cdot \cos(2\tau)}{2} \tag{17}$$

$$\alpha = \frac{k_H \alpha_H + k_V \alpha_V + (k_H \alpha_H - k_V \alpha_V)\cos^2\theta \cos(2\tau)}{2k} \tag{18}$$

where θ is the path elevation angle and τ is the polarization tilt angle relative to the horizontal (45^0 for circular polarization).

IV. BOW-TIE ANTENNA DESIGN

The purpose of this paper is to design a highly directive, low cost, low profile and easily reproducible antenna. This antenna was designed for the use of WLAN 802.11. To achieve this goal we identified four main objectives. The antenna must have high gain, low build cost, small and light weight design, and finally, has to be easy to manufacture.

4.1. Materials and Dimensions

The patch configuration that drives the antenna system to multi-frequency operation is the bowtie shape. Bowtie microstrip antennas are very attractive in present-day communication systems due to their size, which is smaller than the size of a conventional rectangular patch, although they have similar characteristics and they operateat the same frequency. The shape of a bowtie microstrip antenna is shown in Figure 2.

As a substrate material, among plexiglass, FR4, Teflon and Arlon CuClad, the last one has been chosen, because of its properties and cost. The dimensions as shown in Figure 2 are 40x90 mm^2 and the thickness is 2mm. The thicker the substrate material, the higher it costs. The conductive material will be used to produce the microstrip arrays elements, the feed network, and the ground plane. Aluminum and copper were considered and copper has been chosen because of its lower energy loss.
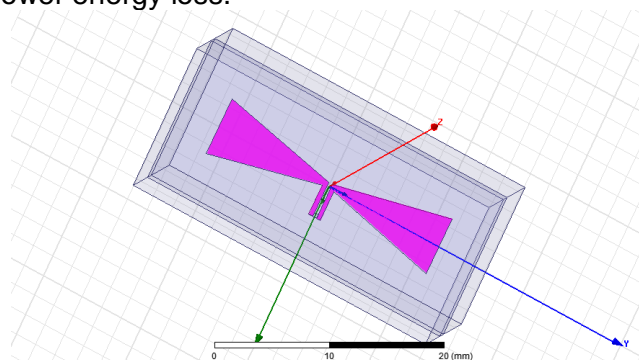
FIGURE 2. The fundamental shape of a bowtie microstrip antenna

The resistance of the transmission line is found by using Equation [7]

$$Z_0 = \frac{87}{\sqrt{\varepsilon_r + 1.41}} \cdot \ln\left(\frac{5.98 \cdot h}{0.8 \cdot W + t}\right) \quad (19)$$

The location of the feed is at the center of the symmetrical microstrip patch design. The antenna is on the above described substrate which has a dielectric constant of 2.17 and the material of the conductor is copper. A radiation box was made to enclose the antenna and a perfectly matched layer (PML) material – an artificial absorbing layer is placed around the box. A parameter sweep was used to determine which height should be used to generate a resonant of approximately 2.4GHz.

The bowtie printed object comes, substantially, from a rectangular patch via modification and the equations for the approximate calculation of the resonance frequency f in terms of the geometrical and material parameter values [17] are:

$$f = \frac{c}{4 \cdot \sqrt{\varepsilon_{eff}}} \cdot \frac{W + W_c + 4 \cdot \Delta L}{3.472 \cdot (W + 2 \cdot \Delta L) \cdot (S + 2 \cdot \Delta L)} \qquad (20)$$

$$\Delta L = \frac{0.412 \cdot h \cdot (\varepsilon_{eff} + 0.3) \cdot \left(\dfrac{W + W_c}{2 \cdot h} + 0.262 \right)}{(\varepsilon_{eff} - 0.258) \cdot \left(\dfrac{W + W_c}{2 \cdot h} + 0.813 \right)} \qquad (21)$$

$$\varepsilon_{eff} = \left(\frac{\varepsilon_r + 1}{2} \right) + \left(\frac{\varepsilon_r - 1}{2} \right) \cdot \sqrt{\frac{W + W_c}{24 \cdot h + W + W_c}} \qquad (22)$$

By altering the dimensions W_c and L and keeping W constant it is possible to change the resonance frequency. The equations given above are a good starting point for the antenna design. However for the best impedance matching, the coordinates of the feed point must be found through iterative simulations. The resonant frequency corresponding to the mode TM_{10} of the equilateral triangular microstrip antenna is [7]

$$f = \frac{4 \cdot c}{3 \cdot L \cdot \sqrt{\varepsilon_r}} \qquad (23)$$

where c is the velocity of light in free space, L is the side length of the bow-tie patch and ε_r is the dielectric constant of the substrate.

The above equation is valid when the triangular resonator is enclosed by a perfect magnetic wall. In case it is not valid, the replacement of side length L by an effective value L_{eff} has been suggested [3], [7], [17]. An approximate expression for L_{eff} produced by curve fitting experimental and theoretical results for the resonant frequency for TM_{10} mode is given by

$$L_{eff} = h \cdot \left(\frac{L}{h} + 4.4 - \frac{25.71}{\sqrt{\varepsilon_r}} + \frac{32.87}{\varepsilon_r} + \frac{24.73 \cdot h}{L} - \frac{39.21 \cdot h}{L \cdot \sqrt{\varepsilon_r}} \right) \qquad (24)$$

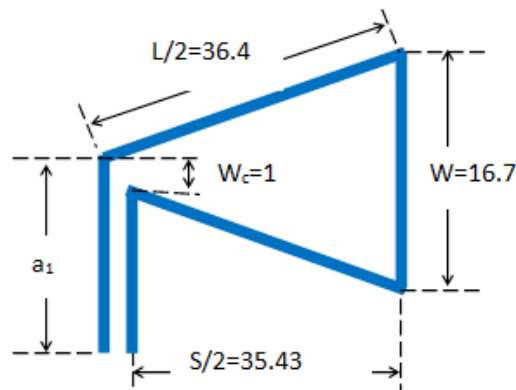where h is the thickness of the substrate.
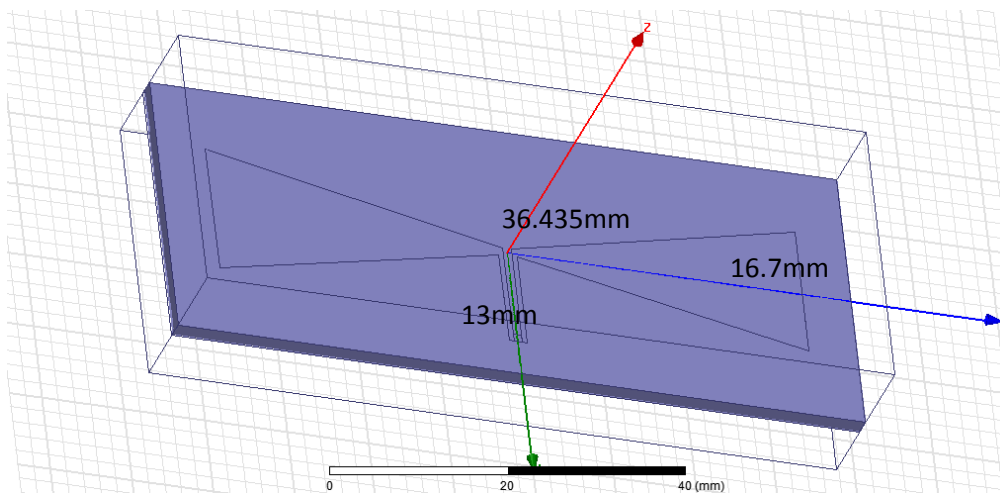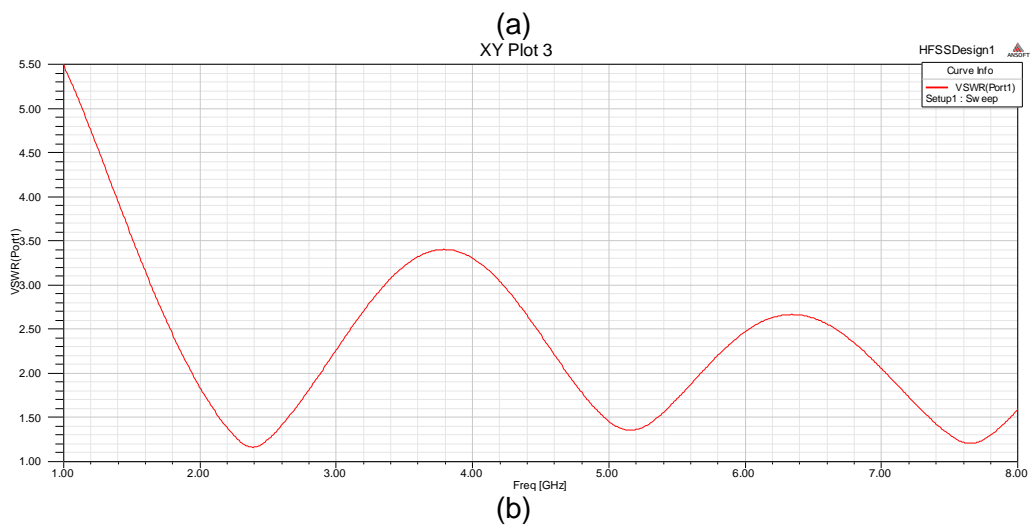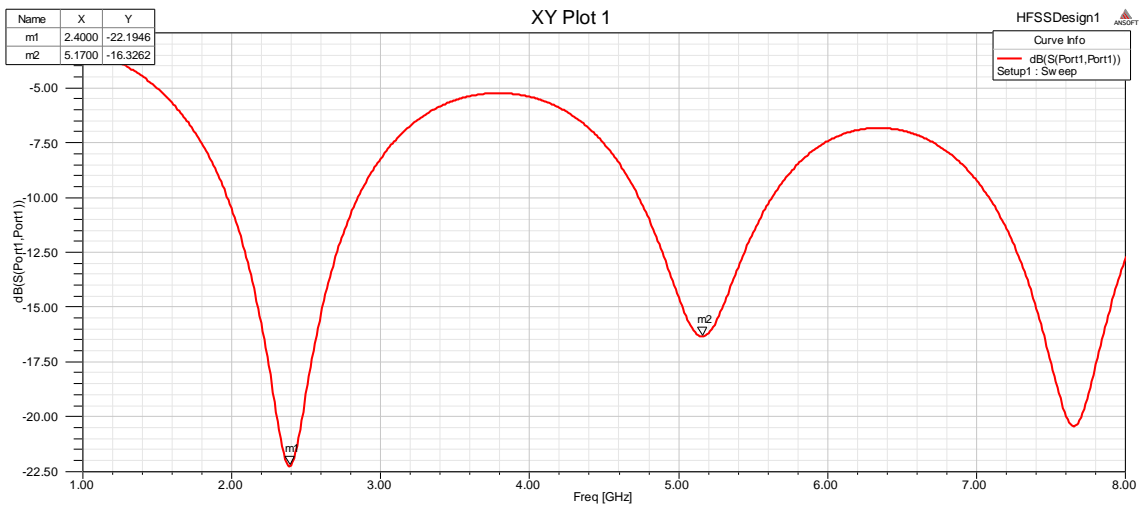

FIGURE 3. Dimensions of the Antenna

FIGURE 4. The Antenna that is simulated

4.2. Simulations

(a)

(b)

(c)

(d)   (e)

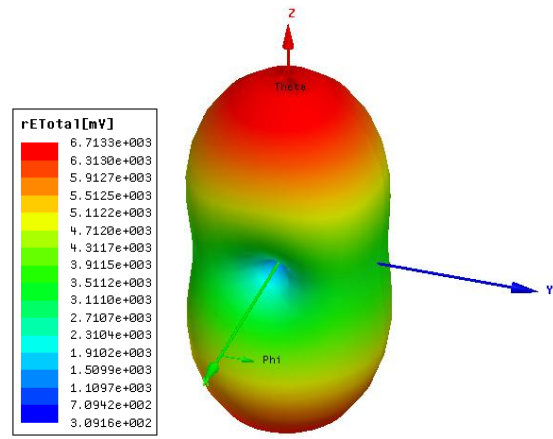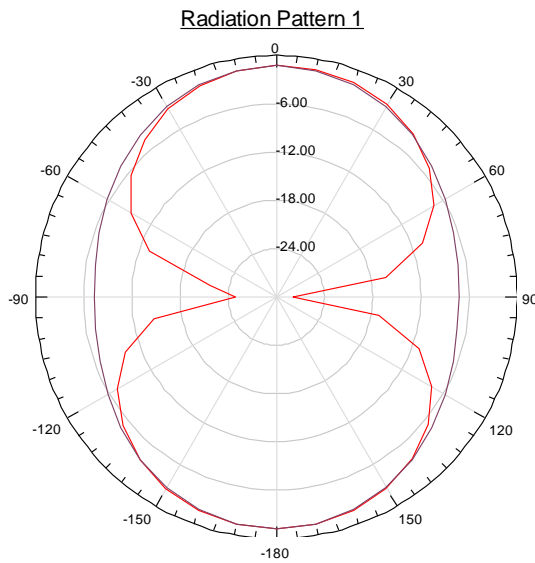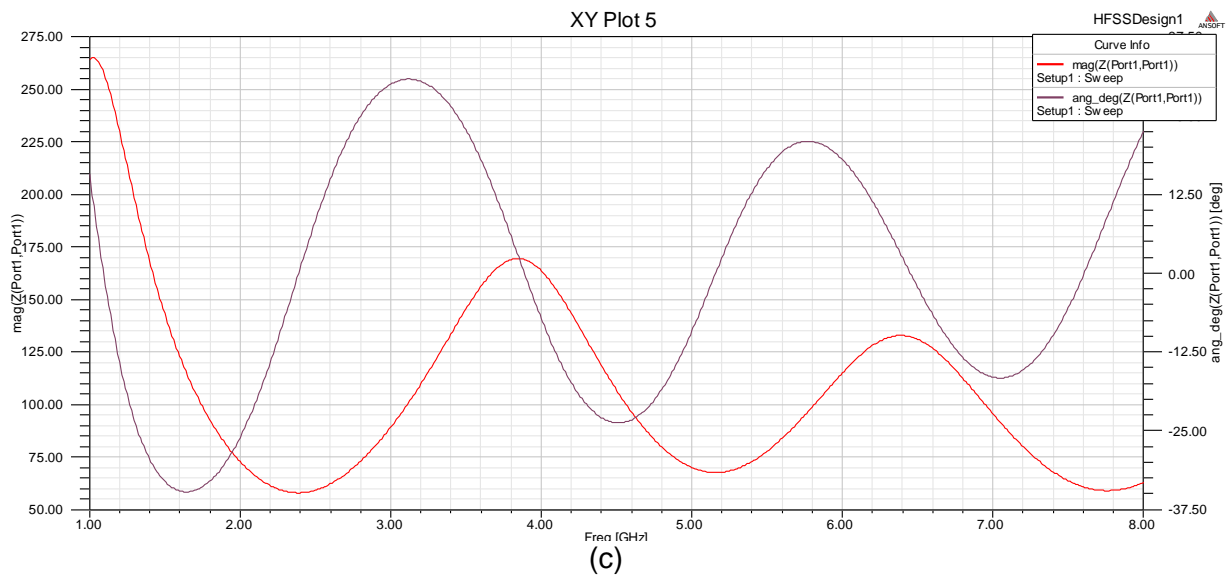**FIGURE 5.** Simulation results for the antenna when works in air (a) Input reflection coefficient, showing that S_{11}=-22dB for f=2.4 GHz and S_{11}=-16 dB for f=5.1 GHz (b) VSWR=1.1 for f=2.4 GHz and VSWR=1.3 for f=5.1 GHz, (c) Magnitude and Angle of the Input Impedance showing that at 2.4 GHz, Z_{IN}=65Ω and at 5.1.GHz is 70 Ω approximately, (d) Radiation Pattern and (e) Directivity

The feeding method depends on the selected bow-tie configuration and the parameter values of the feeding network are calculated by the high frequency transmission microstrip line theory.

V. CONCLUSIONS

In this paper EM waves propagated in troposphere have been discussed. The effect of humidity, has been taken into account in order to characterize the EM wave attenuation. A simple design of a dual band printed antenna functioning in WLAN telecommunication systems, based on the Bow-Tie antenna concept is presented and analyzed by HFSS.
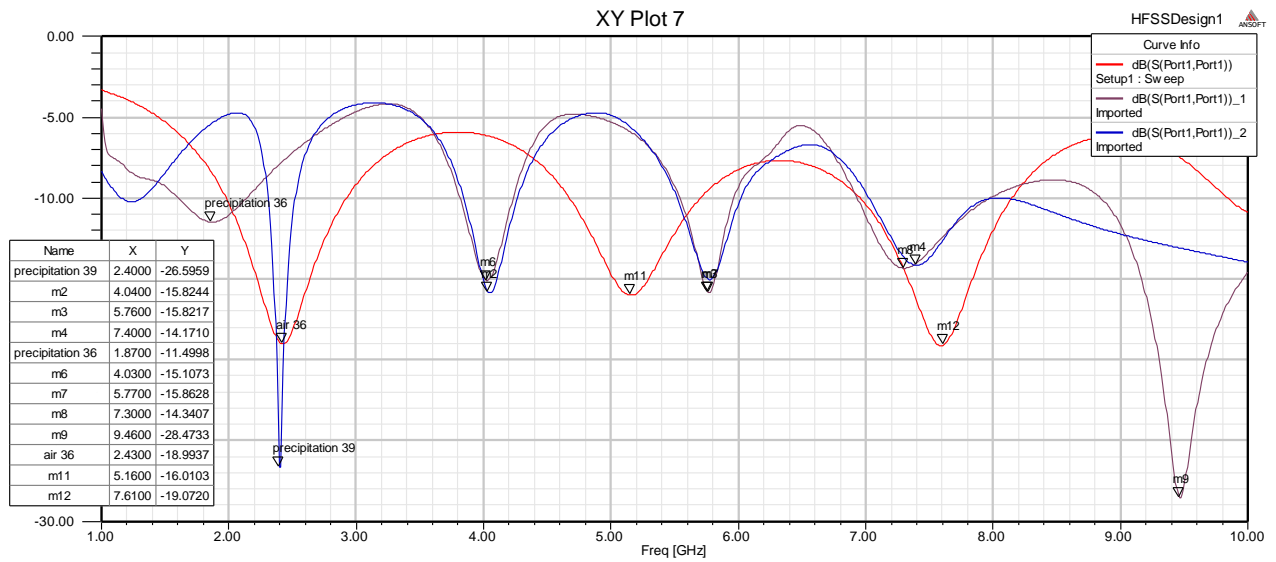
FIGURE 6. Simulation results for the input reflection coefficient of the antenna when works (a) in strong precipitation phenomena with L/2=39mm, (b) in strong precipitation phenomena with L/2=36mm and (c) in air when L/2=36mm

(a) (b)

(c) (d) (e)

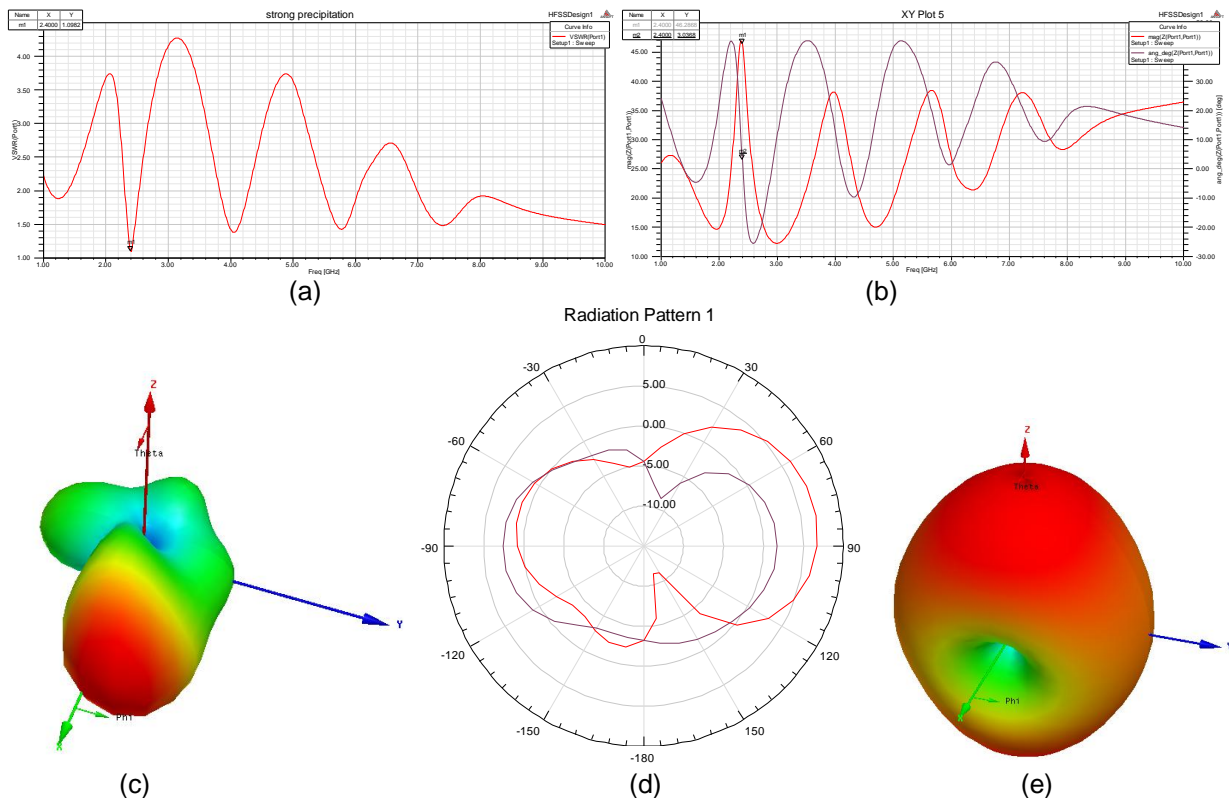**FIGURE 7.** The antenna with L/2=39mm under strong participation (a) VSWR=1.1 for f=2.4 GHz, (b) Magnitude and Angle of the Input Impedance showing that at 2.4 GHz, Z_{IN}=47 Ω and φ=3^0, (c) Directivity, (d) Radiation Pattern and (e) Gain

The antenna design based mainly on the change in the shape of the antenna and its conducting material, the nature and thickness of the substrate that resonates in the frequency desired for specified applications. The optimal variation of each of these parameters affects the resonance frequency, the return loss and the bandwidth of the antenna patch.

The proposed antenna has a wide bandwidth ranging from 2 GHz to 2.7 GHz and 4.7 GHz to 4.6 GHz in air, but in strong precipitation phenomena the bandwidth gets 28% narrower and its dimensions have to be 8% greater in order to work properly at 2.4 GHz. The proposed antennas are of simple structure, easy design, are suitable for the simple 50Ω port feeder, and comply with UWB requirements.

VI. ACKNOWLEDGMENTS

VII. REFERENCES

1. http://www.geekosystem.com/obama-high- speed-wireless-98-percent-americans/
2. J-H. Yoon, "Circular Ring Open-Ended Monopole Antenna with Strip for WLAN Dual-Band Operations" Journal of Information and Communication Convergence Engineering, 2014
3. H. Elsadek, "Microstrip Antennas for Mobile Wireless Communication Systems", Mobile and Wireless Communications: Network layer and circuit level design, InTech, 2010
4. P. Kaur, A. De, S. K. Aggarwal, "Design of A Novel Reconfigurable Fractal Antenna for Multi-Band Application" International Journal of Advanced Science and Technology, 2014
5. K.H. Sayidmarie, Y. A. Fadhel, "A Planar Self-Comlementary Bow-Tie Antenna for UWB Applications" Progress In Electromagnetics Research C, Vol. 35, 253–267, 2013
6. K. Singh, Y. Kumar, S. Singh, "A modified bow tie antenna with U-shape slot for Wireless applications", International Journal of Emerging Technology and Advanced Engineering, Volume 2, Issue 10, 2012
7. K. Siakavara, "Methods to Design Microstrip Antennas for Modern Applications", Microstrip Antennas, InTech, 2011
8. S. Uysal, M.-S.Leong, C.Hong Ng, "Bowtie Patch Antennas and Simple Arrays for Wireless Indoor Communications", IEEE Transactions on Microwave Theory and Techniques, Vol. 47, No. 6, 1999
9. S. Srivastava and V. K. Singh, "Bow-Tie Shaped Printed Antenna for UMTS/WLAN/WiMAX Applications", Journal of Environmental Science, Computer Science and Engineering & Technology, 2013
10. Y. Tawk, K. Y. Kabalan, A. El-Hajj, C. G. Christodoulou, J. Costantine, "A Simple Multiband Printed Bowtie Antenna", IEEE Antennas and Wireless Propagation Letters, Vol. 7, 2008
11. IEEE Standard 802.11, 2012
12. S. Makarov, "Antennas", Worcester Polytechnic Institute, USA, John Wiley & Sons, 2011
13. IEEE, "IEEE Standard Definitions of Terms for Antennas," IEEE, pp. 0-1, February 1983
14. C. Fung, "Basic Antenna Theory and Application", Worcester Polytechnic Institute, 2011
15. A. Eldek, A. Z. Elsherbeni, C. E. Smith, "Wideband Microstrip-Fed, Printed Bow Tie Antenna for Phased-Array Systems", Microwave and Optical Technology Letters, Vol. 43, No. 2, 2004
16. M. Iftissane, S. Bri, L. Zenkouar, A. Mamouni, "Conception of Patch Antenna at Wide Band", Int. J. Emerg. Sci., 400-417, 2011

17. C. Balanis, Antenna Theory: Analysis and Design, 3rd ed. Hoboken, United States of America: Wiley-Interscience, 2005

18. Sergey Makarov, Selected Lectures - Antennas. Worcester, United States of America: John Wiley & Sons Inc, 2011

19. A. Ghasemi, A. Abedi, F. Ghasemi, "Propagation Engineering in Wireless Communications", Springer New York, 2012

20. Rinehart, R. E., "Radar for Meteorologists", 3rd Edition, Rinehart Publications, Grand Forks, 1997

21. G.D.Thayer, "An Improved Equation for the Radio Refractive Index of Air." Radio Science, Vol. 9, No. 10, 1974

22. S.P. Mason, "Atmospheric Effects on Radio Frequency (RF) Wave Propagation in a Humid Near-Surface Environment", Naval Postgraduate School, Monterey, California, 2010

23. S.Q. Kidder, S.H. Vonder Haar, "Satellite Meteorology: An Introduction", Academic Press, New York, 1995

24. R.A. Helvey, J.S. Rosenthal, "Guide for Inferring Refractive Conditions from Synoptic Parameters," Technical Report, Pacific Missile Test Center, 1983

25. C.C. Chen, "Attenuation of Electromagnetic Radiation by Haze, Fog, Clouds and Rain", Rand Corporation, United States Air Force Project Rand, 1975

26. J. Bech, A. Magaldi, B. Codina, J. Lorente, "Effects of Anomalous Propagation Conditions on Weather Radar Observations"

27. J. Bech and J.-L. Chau, "Doppler Radar Observations - Weather Radar, Wind Profiler, Ionospheric Radar, and Other Advanced Applications", InTech, 2012

28. E.A. Karagianni, "Electromagnetic Waves under Sea: A Bow-Tie Antenna Design for Wi-Fi Underwater Communications", Progress In Electromagnetics Research M, Vol. 41, 189–198, 2015

29. G.Penn, J.-L. Vay, "Theoretical Studies of TE-Wave Propagation as a Diagnostic for Electron Cloud", Proceedings of IPAC'10, Kyoto, Japan, 2010

30. R.Barra, D.Llanwyn Jones, C.J. Rodgerc, "ELF and VLF radio waves", Journal of Atmospheric and Solar-Terrestrial Physics 62, 2000

31. P. Devine, "Radar level measurements, The user's guide", VEGA Controls, 2000

32. S. Tamosiunas, M. Tamosiunaite, M. Zilinskas, and M. Tamosiuniene, "The Influence of Fog on the Propagation of the Electromagnetic Waves under Lithuanian Climate Conditions", PIERS online, Vol.5, No.6, 2009

33. R. Milione, "Fundamentals of RF Propagation in Electronic Warfare", Institute for Defence and Government Advancement, 2011

34. O. Sirkova, M. Mikhalev, "Parabolic Wave Equation Method Applied to the Tropospheric Ducting Propagation Problem: A Survey", Electromagnetics, 26:155–173, 2006

35. Johnson, R. H., Rickenbach, T. M., Rutledge, S. A., Ciesielski, P. E., and Schubert, W. H., "Trimodal characteristics of tropical convection", J. Climate, 12, 2397-2418, 1999.

36. Papatsoris, K. Polimeris, I. Sklari, A. Lazou, "Rainfall Characteristics for Radiowave Propagation Studies in Greece", Antennas and Propagation Society International Symposium, 2008

37. B. Segal, "The Infuence of Raingage Integration Time on Measured Rainfall-Intensity Distribution Functions", Journal of Atmospheric and Oceanic Technology, Vol. 3, 1986

38. R.H.Johnson, T.M. Rickenbach, S.A. Rutledge, P.E. Ciesielski, W.H. Schubert, "Trimodal characteristics of tropical convection", J. Climate, 12, 2397-2418, 1999.

39. Recommendation ITU-R, P.838-3, Specific attenuation model for rain for use in prediction methods

40. P. A. Owolawi, T. J. Afullo, and S. B. Malinga, "Effect of Rainfall on Millimeter Wavelength Radio in Gough and Marion Islands", Progress In Electromagnetics Research Symposium, Beijing, China, March 23–27, 2009